

Research



Cite this article: Mughal EU *et al.* 2020

Terpyridine-metal complexes: effects of different substituents on their physico-chemical properties and density functional theory studies. *R. Soc. Open Sci.* **7**: 201208.

<http://dx.doi.org/10.1098/rsos.201208>

Received: 28 July 2020

Accepted: 7 October 2020

Subject Category:

Chemistry

Subject Areas:

chemical biology

Keywords:

terpyridine, fluorescence, anti-microbial activity, molecular docking, density functional theory, structure–activity relationship

Authors for correspondence:

Ehsan Ullah Mughal

e-mail: ehsan.ullah@uog.edu.pk

Masoud Mirzaei

e-mail: mirzaeesh@um.ac.ir

This article has been edited by the Royal Society of Chemistry, including the commissioning, peer review process and editorial aspects up to the point of acceptance.

Electronic supplementary material is available online at <https://dx.doi.org/10.6084/m9.figshare.c.5215947>.



Terpyridine-metal complexes: effects of different substituents on their physico-chemical properties and density functional theory studies

Ehsan Ullah Mughal¹, Masoud Mirzaei², Amina Sadiq³, Sana Fatima¹, Ayesha Naseem¹, Nafeesa Naeem¹, Nighat Fatima⁴, Samia Kausar¹, Ataf Ali Altaf^{1,5}, Muhammad Naveed Zafar⁶ and Bilal Ahmad Khan⁷

¹Department of Chemistry, University of Gujarat, Gujarat 50700, Pakistan

²Department of Chemistry, Faculty of Science, Ferdowsi University of Mashhad, PO Box 9177948974, Mashhad, Iran

³Department of Chemistry, Government College Women University, Sialkot 51300, Pakistan

⁴Department of Pharmacy, COMSATS University Islamabad, Abbottabad Campus, 22060, Pakistan

⁵Department of Chemistry, University of Okara, Okara 56300, Pakistan

⁶Department of Chemistry, Quaid-i-Azam University, Islamabad 45320, Pakistan

⁷Department of Chemistry, University of Azad Jammu and Kashmir, Muzaffarabad, Pakistan

MM, 0000-0002-7256-4601; AAA, 0000-0001-8018-5890

A series of different substituted terpyridine (tpy)-based ligands have been synthesized by Kröhnke method. Their binding behaviour was evaluated by complexing them with Co(II), Fe(II) and Zn(II) ions, which resulted in interesting coordination compounds with formulae, $[Zn(tpy)_2]PF_6$, $[Co(tpy)_2](PF_6)_2$, $[Fe(tpy)_2](PF_6)_2$ and interesting spectroscopic properties. Their absorption and emission behaviours in dilute solutions were investigated in order to explain structure–property associations and demonstrate the impact of different aryl substituents on the terpyridine scaffold as well as the role of the metal on the complexes. Photo-luminescence analysis of the complexes in acetonitrile solution revealed a transition from hypsochromic to bathochromic shift. All the compounds displayed remarkable photo-luminescent properties and various maximum emission peaks owing to the different nature of the functional groups. Furthermore, the anti-microbial potential of ligands and complexes was evaluated with docking analyses carried out to investigate the binding affinity of terpyridine-based ligands along with corresponding proteins (shikimate dehydrogenase

and penicillin-binding protein) binding sites. To obtain further insight into molecular orbital distributions and spectroscopic properties, density functional theory calculations were performed for representative complexes. The photophysical activity and interactions between chromophore structure and properties were both investigated experimentally as well as theoretically.

1. Introduction

2,2':6',2''-Terpyridine is a tridentate ligand which contains three coordination sites belonging to *N*-heteroaromatic rings (figure 1) and thus constitutes a significant class of aromatic heterocyclic compounds. Owing to their strong chelating tendency, these ligands can form stable complexes with several different main groups and transition metal ions. In the past, terpyridine motifs and their complexes have attracted the increasing attention of materials chemists due to their applications in several fields, for instance photovoltaic devices, DNA binders, sensors, photosensitizers, molecular chemistry, medicinal chemistry and metal-organic framework (MOF) construction [1–3].

Moreover, their complexes with transition metals, in particular, can lead to unique photo-luminescence, catalysis, sensor properties and quite promising tumour-inhibiting activities [4–19]. Due to environmental and economic considerations, increasing attention has been paid to the development of such compounds for use in many fields, especially in medicinal and material chemistry. Constable's group has thoroughly studied the synthesis of terpyridine derivatives, and a wide variety of substituted terpyridine ligands were prepared in high yields through the Kröhnke reaction by condensation of 2-acetylpyridine with various substituted aryl aldehydes followed by oxidation in simple and effective processes [20–25]. These ligands show unique coordinative capabilities towards transition elements and have received much attention recently because of their varied/extensive uses in diverse research fields extending from therapeutic uses (such as anti-cancer and DNA intercalation) to material sciences (photovoltaics, sensitizers) and catalysis [26]. Supramolecular chemistry and material science are another field where 2,2':6',2''-terpyridines and their derived complexes are widespread and used as significant organic ligands [27–30]. The features of the metal-containing assemblies depend on the electronic impact of both the terpyridine unit and its substituents as well as the metal ion [31]. These compounds provide an opportunity to probe the effects of the ligand, the central metal ion and the coordination geometry on the binding properties. 2,2':6',2''-Terpyridine and its structural derivatives with prolific coordination chemistry were broadly considered for their strong binding affinity for a variety of transition metal ions resulting in various metal supramolecular architectures with fascinating photophysical and redox characteristics [32–36]. Hofmeier *et al.* [34] and Alcock *et al.* [12] have synthesized ligands based on terpyridine and developed radiative metallo-supramolecular coordination compounds accumulated through π - π fibre optics in which violet-blue emissions are ascribed to π - π fibre optic ligand transfer. It has been shown that a donor-acceptor system is an efficient approach for adapting the optical properties of organic-inorganic hybrid materials [37,38]. Moreover, transition metal complexes give many advantages, for example, long-lived fluorescent excited states and photochemical strengths [39]. Furthermore, the core-functionalization of terpyridine units with electron-donating/withdrawing substituents has not been developed as much as possible fluorescent probes. The studies indicated that electron-accepting and -donating substituents may be used to modify the photophysical and oxidation-reduction properties of free terpyridines and their metal complexes [40]. Therefore, to obtain more knowledge of the structure-activity correlation (absorption and emission properties), a great variety of substituents having different electron-releasing or -accepting behaviour were introduced on the *p*-position of the terpyridine rings.

Furthermore, there has been recent interest in the terpyridine moiety, not only because of its exciting molecular topologies in the design and synthesis of polymers for coordination but also because they have strong anti-microbial activity, which could provide an important point of reference for more effective anti-microbial drug design [41–48]. This increased lipophilicity can lead to a breakdown of the cell permeability barrier, thereby blocking normal cell processes [49–52]. Previous studies [53,54] showed that bidentate or tridentate ligands with greater lipophilicity had higher anti-microbial activity than monodentate ligands and, as stated by the principle of similarity and inter-miscibility, two different types of ligands in complexes had stronger anti-bacterial activity than a single ligand. It would be motivated to discover the structure-property relationship between complex structures and anti-microbial properties, which can offer theoretical directions for designing and synthesizing complexes with useful biological activities [55–64].

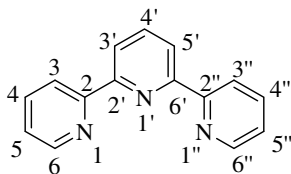


Figure 1. Structural representation of terpyridine framework.

Based on the aforementioned considerations, we report the design, synthesis and characterization of variously functionalized terpyridine ligands and their Zn(II), Co(II), and Fe(II) complexes. Thorough photophysical and computational studies of the new complexes provide an insight into their electronic structure, which provides a significant extension of newly published terpyridine-transition metal complexes. In addition, we have established a detailed structure–activity relationship (SAR) between these architectures and their biological and spectrophotometric properties.

2. Materials and methods

All chemicals were bought from Merck and Sigma-Aldrich and used as received. Melting points have been recorded with an electrothermal device and are uncorrected. The FTIR spectra have been obtained on a Bio-Rad spectrophotometer and the infrared values are listed in $\bar{\nu}$ units. The UV-Vis spectra were recorded in chloroform (CHCl_3) and acetonitrile (CH_3CN) solutions, respectively, on a Jasco UV-Vis V-660 instrument using a QUARTZ cell. The luminescence spectra were obtained using a Shimadzu 8101AFT-IR instrument. Thin-layer chromatography (TLC) was conducted on silica gel TLC plates purchased from Merck and chromatograms were viewed with a UV-lamp at 254 and 365 nm.

2.1. General procedure for the synthesis of 4'-substituted terpyridine ligands and complexes

2.1.1. Synthesis of ligand (4'-aryl-substituted 2,2':6',2''-terpyridine) [65]

To a mixture of 2-acetylpyridine (2.43 g, 20.0 mmol) in methanol (20 ml), a substituted aryl aldehyde (10.0 mmol) was added, followed by potassium hydroxide (KOH) pellets (1.54 g, 24 mmol) and 35% aqueous ammonia solution (40.0 ml). The reaction mixture was refluxed for 4–6 h. After the reaction was completed (determined by TLC monitoring), the solvent was removed under vacuum and the precipitates were filtered, washed with plenty of distilled H_2O to remove the excess base and finally with ice-cold EtOH until the washings were neutral. The residue was dried in the open air and recrystallized from ethanol.

2.1.2. Synthesis of terpyridine metal complexes (C_1 – C_{27}) [66]

A hot methanolic solution (20.0 ml) of metal salt (0.5 mmol) was introduced dropwise to a CH_2Cl_2 solution (20.0 ml) of the substituted terpyridine ligand (0.28 g, 1.0 mmol) under continuous stirring. The colour of the reaction mixture instantly changed and the reaction mixture was stirred for approximately 2 h at room temperature. Upon addition of an excess of NH_4PF_6 precipitation occurred. The precipitates were filtered, washed with ice-cold MeOH (5.0 ml) and $(\text{C}_2\text{H}_5)_2\text{O}$ (15.0 ml) to obtain a pure complex. Recrystallization from acetonitrile or methanol or a mixture of both yielded the analytically purified complex.

2.2. Photo-luminescence studies

RF-6000 Spectrofluorophotometer was used to produce an emission spectrum for ligands and their complexes. The emission spectra of the synthesized ligand in chloroform and of complexes in acetonitrile were obtained by using a fluorescence spectrophotometer. The emission spectra were checked by keeping the excitation value of the synthesized compounds at 325 nm [40,67–72]. The fluorescence spectra have been observed at 335 nm for ligands (L_1 – L_9) and 520 nm for complexes (C_1 – C_{27}).

2.3. Molecular docking studies

2.3.1. Accession of targets proteins

Chemical structures of the terpyridines were developed with ChemBio Draw which also produced their MOL format files. The shikimate dehydrogenase (PDB ID: 3DON) and penicillin-binding protein (PDB ID: 1VQQ) three-dimensional crystal structures have been accessed and downloaded from the protein data bank database (PDB) [<http://www.rcsb.org/pdb/home/home.do>] [71].

2.3.2. Analysis of target active binding sites

The active sites of the target protein were examined using the molecular operating environment (MOE) software. An active site was distinct from the ligand coordinates in the original protein sites [40,72–75].

2.3.3. Docking analysis

A theoretical ligand-target docking method has been used to classify structural complexes of the shikimate dehydrogenase crystal structure and penicillin-target protein with ligand molecules to recognize the molecular basis of the specificity of these protein targets. Eventually, the MOE program performs docking. The energy of these derivatives to interact with the protein targets is given 'grid level'.

2.4. Density functional theory studies

Computational calculations were performed by using DFT-B3LYP*(DZ) in the Amsterdam Density Functional (ADF) modelling suite [76]. The ground states geometries of metal complexes (**C**₁₃, **C**₁₄, **C**₁₅, **C**₂₂, **C**₂₃ and **C**₂₄) were optimized using the B3LYP* hybrid functional and double zeta (DZ) basis sets.

2.5. Anti-microbial studies

2.5.1. Anti-bacterial activity

All the new compounds were assessed using a disc-diffusion method for the *in vitro* anti-bacterial activity against Gram-negative *Escherichia coli* (ATCC 25922) and *Pseudomonas aeruginosa* (ATCC 9721) and Gram-positive *Staphylococcus aureus* (ATCC 6538) bacterial strains. Cefixime was used as a positive standard and dimethyl sulfoxide (DMSO) as a negative control. Various sample solutions were prepared by dissolving 4.0 mg of each sample in 1.0 ml of DMSO. The lawn was developed on nutrient agar plates using bacterial strains of equal turbidity that is accomplished using 0.5% of McFarland's solution. The well depth was 8 mm and they were all made at the correct distances from each other. The sample and standard are poured into their respective tubes. The sample quantity used was 80 µl in a well together with the two controls. The prepared dishes were incubated for 24 h at 37°C, and the findings were reported as the average diameter of zone of inhibition (ZOI) of bacterial development around the discs in millimetres for each compound [75,77].

2.6. Anti-fungal activity

The new compounds have also been tested for anti-fungal activity, using the process of well diffusion [75,77]. Two fungal strains were used for these experiments: one *Candida albicans* (ATCC 9002) and a second *Candida parapsilosis* (ATCC 22019). To relate the activities of target compounds, clotrimazole (1 mg ml⁻¹ in DMSO) was used as a standard. The inhibition zone was calculated to obtain quantitative activity information. The sample solutions were prepared by adding 4.0 mg of sample in 1.0 ml solvent (DMSO). Using a sterile glass rod, a spore suspension aliquot (1108 spores ml⁻¹) was spread evenly over Sabouraud dextrose agar (SDA). Eight-millimetre diameter wells were built at suitable ranges. An 80 µl aliquot of sample was introduced into each well using a micropipette and the loaded plates were incubated at 28°C for 24–28 h. Anti-fungal behaviour was measured as the circular diameter of the zone of inhibition in millimetres.

3. Results and discussion

3.1. Chemistry

The synthesis of terpyridine ligands (**L**₁–**L**₉) was carried out by Kröhnke method [65]. Our preliminary study focused on the synthesis of different 6,6'' symmetrically substituted 4'-aryl-2,2':6',2''-terpyridine

substrates. As outlined in scheme 1, the aromatic aldehydes were condensed with 2-acetylpyridine in the presence of methanolic-potassium hydroxide and aqueous ammonia solution to furnish terpyridine ligands (**L**₁–**L**₉) in moderate to excellent yields. Purification of the ligands was achieved by recrystallization from ethanol. The chemical structures of all the ligands were corroborated by UV-Vis, FTIR and NMR spectroscopies. Subsequently, these ligands were coordinated with the transition metal cations Fe²⁺, Co²⁺, Zn²⁺ to produce the desired complexes (**C**₁–**C**₂₇) in very good yields. These complexes were prepared by the reaction of the terpyridine ligands with the metal salts in a 2:1 molar ratio in dichloromethane (DCM) and purified by washing with ethanol. The ligands (**L**₁–**L**₉) and their complexes (**C**₁–**C**₂₇) are stable at ambient temperature and readily soluble in chloroform and/or acetonitrile. Characterization of the complexes was accomplished from their FTIR and ¹H NMR and ¹³C NMR spectra. The FTIR spectra were acquired over the 4000–400 cm⁻¹ range. For ligands (**L**₁–**L**₉), characteristic bands in the regions 3013–3062 and 1597–1660 cm⁻¹ are assigned to ν_{C–H} and ν_{C=N} stretching vibrations, respectively. The bands in the region 1443–1530 cm⁻¹ are due to C=C stretching vibration, and the band in the range 1240–1358 cm⁻¹ is assigned to the C–N group, but in the case of metal complexes (**C**₁–**C**₂₇), the C–H group disappeared. Moreover, the presence of a strong absorption peak in the 1587–1615 cm⁻¹ range is attributed to the azomethine moiety indicating the formation of a –CH=N bond. However, on complexation, the characteristic ν(C=N) band was shifted towards the lower frequency suggesting coordination of the metal with the terpyridine moiety in the ligand framework.

The electronic absorption spectra of the compounds were recorded in the 200–800 nm range in chloroform and acetonitrile solutions. The compounds show absorption bands in the 234–350 nm range which may be assigned to π–π* energy transitions of the C=N and phenyl moieties. Finally, coordination of the new ligands with various metal cations and the molar masses of the resulting complexes were confirmed by MALDI mass spectrometers. Spectroscopic data are in good agreement with the proposed structures of all ligands as well as complexes. Unfortunately, various attempts to grow a single crystal of the complexes for X-ray diffraction analysis proved unsuccessful.

The physical and spectroscopic data of all the new ligands and complexes are given below:

3.2. 4'-(4-Methylphenyl)-2,2':6',2''-terpyridine (**L**₁) [68]

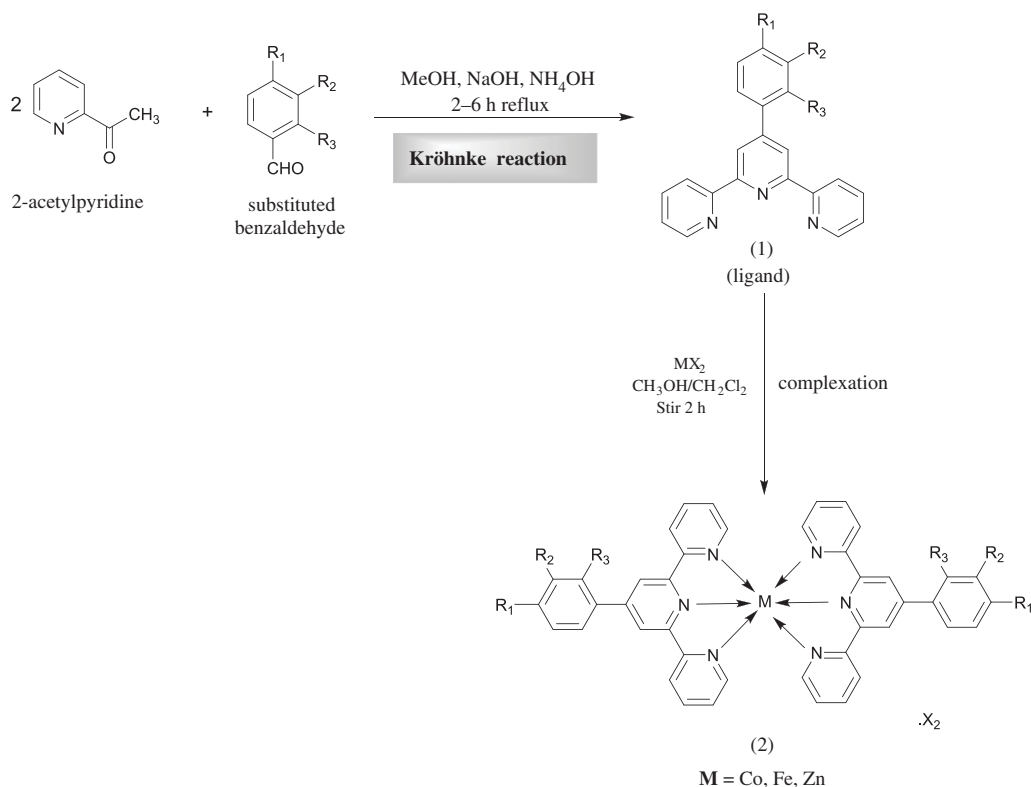
Colourless crystalline solid; Yield: 62%; m.p. 162–167°C; UV λ_{max} (CHCl₃) = 325 nm; λ_{em} (CHCl₃): 357, 731 nm; FTIR (cm⁻¹): 3013 (C–H), 1601 (C=N), 1464 (C=C), 1311 (C–N), 1257 (C–H), 1066 (C–H); ¹H NMR (300 MHz, CDCl₃) δ 8.73–8.70 (m, 4H, Ar–H), 8.65 (d, *J* = 9.0 Hz, 2H, Ar–H), 7.86–7.84 (m, 4H, Ar–H), 7.84 (d, *J* = 9.0 Hz, 2H, Ar–H), 7.35–7.30 (m, 2H, Ar–H), 2.42 (s, 3H, –CH₃); ¹³C NMR (75 MHz, CDCl₃) δ 156.4, 156.0, 151.2, 150.0, 137.0, 134.3, 130.0, 128.2, 124.0, 121.5, 118.8, 21.3, other carbons are isochronous.

3.3. *N,N*-dimethyl-4-(2,2':6',2''-terpyridin-4'-yl)aniline (**L**₂) [78]

Green amorphous solid; Yield: 71%; m.p. 180–195°C; UV λ_{max} (CHCl₃) = 293 nm; λ_{em} (CHCl₃): 344, 443 nm; FTIR (cm⁻¹): 2809 (C–H), 1595 (C=N), 1464 (C=C), 1358 (C–N), 1190 (C–H), 1045 (C–H); ¹H NMR (300 MHz, CD₃CN) δ 8.70 (d, *J* = 9.0 Hz, 2H, Ar–H), 8.52–8.45 (m, 4H, Ar–H), 8.31 (d, *J* = 9.0 Hz, 2H, Ar–H), 7.93 (s, 2H, Ar–H), 7.93–7.82 (m, 1H, Ar–H), 7.50–7.48 (m, 1H, Ar–H), 7.24–7.19 (m, 1H, Ar–H), 7.08–7.03 (m, 1H, Ar–H), 3.46 (s, 6H, –CH₃); ¹³C NMR (CD₃CN, 75 MHz) δ 160.0, 159.4, 157.3, 156.3, 154.8, 153.5, 152.9, 138.6, 138.5, 135.2, 128.3, 127.7, 125.0, 124.7, 124.3, 107.4, 40.8, other carbons are isochronous.

3.4. *N,N*-diphenyl-4-(2,2':6',2''-terpyridin-4'-yl)aniline (**L**₃)

Yellow amorphous solid; Yield: 75%; m.p. 160–162°C; UV λ_{max} (CHCl₃) = 234 nm; λ_{em} (CHCl₃): 335, 576 nm; FTIR (cm⁻¹): 3054 (C–H), 1660 (C=N), 1565 (C=C), 1271 (C–N), 1120 (C–H); ¹H NMR (300 MHz, Acetone-*d*₆) δ 9.03 (bs, 1H, Ar–H), 8.87 (d, *J* = 9.0 Hz, 1H, Ar–H), 8.62–8.56 (m, 1H, Ar–H), 8.37 (d, *J* = 9.0 Hz, 2H, Ar–H), 8.11–7.97 (m, 3H, Ar–H), 7.90–7.85 (m, 1H, Ar–H), 7.72–7.67 (m, 2H, Ar–H), 7.55–7.47 (m, 2H, Ar–H), 7.27 (t, *J* = 9.0 Hz, 2H, Ar–H), 7.14–7.01 (m, 4H, Ar–H), 6.88 (d, *J* = 9.0 Hz, 2H, Ar–H); ¹³C NMR (75 MHz, Acetone-*d*₆) δ 162.7, 156.7, 156.2, 147.4, 147.1, 138.1, 130.7, 130.3, 129.7, 129.6, 129.5, 128.4, 126.8, 126.3, 125.5, 125.4, 124.6, 122.4, 121.1, 118.4, other carbons are isochronous.



Scheme 1. Synthetic routes to the ligands (**L₁–L₉**) and their complexes (**C₁–C₂₇**).

3.5. 4'-(4-Methoxyphenyl)-2,2':6',2''-terpyridine (**L₄**) [79,80]

Dark-brown amorphous solid; Yield: 62%; m.p. 162–164°C; UV λ_{\max} (CHCl₃) = 248 nm; λ_{em} (CHCl₃): 371, 746, 855 nm; FTIR (cm⁻¹): 3024 (C-H), 1689 (C=N), 1466 (C=C), 1305 (C-N), 1236 (C-H), 1150 (C-H); ¹H NMR (300 MHz, CDCl₃) δ 8.65–8.54 (m, 4H, Ar-H), 8.50 (d, J = 9.0 Hz, 2H, Ar-H), 7.80–7.82 (m, 4H, Ar-H), 7.83 (d, J = 9.0 Hz, 2H, Ar-H), 7.32–7.29 (m, 2H, Ar-H), 3.9 (s, 3H, -OCH₃); ¹³C NMR (75 MHz, CDCl₃) δ 156.4, 156.0, 151.2, 150.0, 137.0, 134.3, 130.0, 128.2, 124.0, 121.5, 118.8, 54.2, other carbons are isochronous.

3.6. 4'-(3-Trifluoromethylphenyl)-2,2':6',2''-terpyridine (**L₅**)

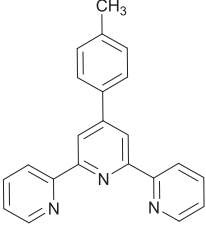
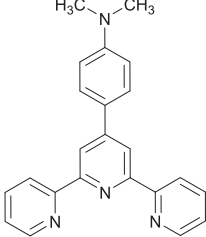
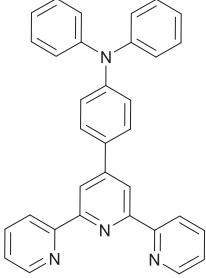
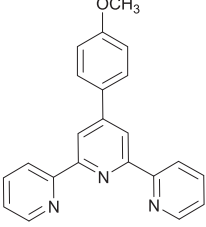
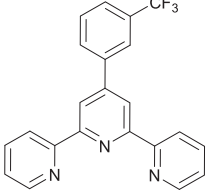
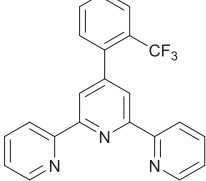
Off-white crystalline solid; Yield: 70%; m.p. 135–136°C; UV λ_{\max} (CHCl₃) = 234 nm; λ_{em} (CHCl₃): 359, 727, 861 nm; FTIR (cm⁻¹): 3356 (C-H), 1604 (C=N), 1454 (C=C), 1281 (C-N), 1152 (C-H); ¹H NMR (300 MHz, CDCl₃) δ 8.31–8.28 (m, 4H, Ar-H), 8.24–8.21 (m, 2H, Ar-H), 7.69 (s, 1H, Ar-H), 7.64 (d, J = 9.0 Hz, 1H, Ar-H), 7.47 (ddd, J = 3.0, 6.0, 9.0 Hz, 2H, Ar-H), 7.29 (d, J = 9.0 Hz, 1H, Ar-H), 7.22–7.17 (m, 1H, Ar-H), 6.94–6.90 (m, 2H, Ar-H); ¹³C NMR (75 MHz, CDCl₃) δ 156.4, 156.0, 155.6, 149.1, 148.8, 139.0, 137.0, 136.9, 130.7, 130.4, 130.1, 129.3, 126.0, 125.6, 125.4, 124.1, 124.0, 121.4, 121.2, 118.5, 77.4,

3.7. 4'-(2-Trifluoromethylphenyl)-2,2':6',2''-terpyridine (**L₆**) [81]

Light-yellow crystalline solid; Yield: 64%; m.p. 148–150°C; UV λ_{\max} (CHCl₃) = 240 nm; λ_{em} (CHCl₃): 345, 70, 80 nm; FTIR (cm⁻¹): 3362 (C-H), 1655 (C=N), 1493 (C=C), 1311 (C-N), 1280 (C-H), 1150 (C-H); ¹H NMR (300 MHz, CDCl₃): δ 8.72–8.70 (m, 4H, Ar-H), 8.54 (s, 2H, Ar-H), 7.84–7.77 (m, 2H, Ar-H), 7.54–7.49 (ddd, J = 3.0, 6.0, 9.0 Hz, 2H, Ar-H), 7.35 (d, J = 9.0 Hz, 2H, Ar-H), 7.25–7.20 (m, 2H, Ar-H); ¹³C NMR (75 MHz, CDCl₃) δ 156.3, 156.1, 155.5, 150.0, 149.0, 139.0, 137.1, 137.0, 130.6, 131.0, 130.0, 129.2, 126.1, 125.5, 125.4, 124.1, 123.8, 121.2, 121.0, 118.4, 77.3.

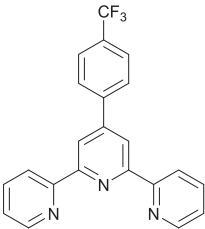
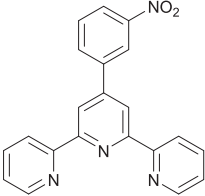
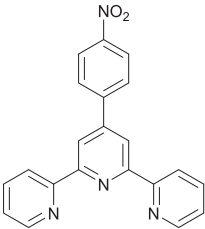
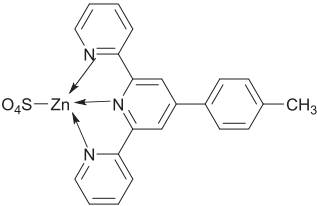
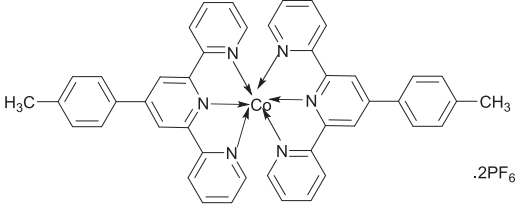
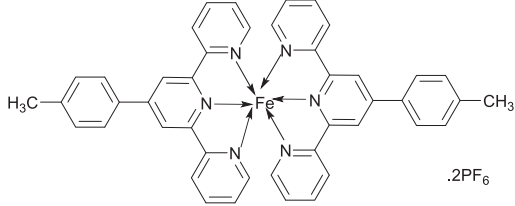
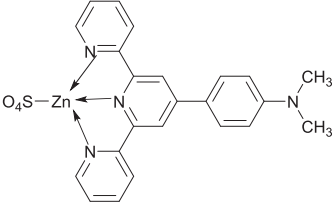
3.8. 4'-(4-Trifluoromethylphenyl)-2,2':6',2''-terpyridine (**L₇**)

Off-white amorphous solid; Yield 68%; m.p. 129–131°C; UV λ_{\max} (CHCl₃) = 234 nm; λ_{em} (CHCl₃): 345, 723, 852 nm; FTIR (cm⁻¹): 3361 (C-H), 1619 (C=N), 1469 (C=C), 1326 (C-N), 1261 (C-H), 1143 (C-H); ¹H NMR (300 MHz, CDCl₃) δ 8.66–8.63 (m, 4H, Ar-H), 8.61–8.58 (m, 2H, Ar-H), 7.93 (d, J = 9.0 Hz,

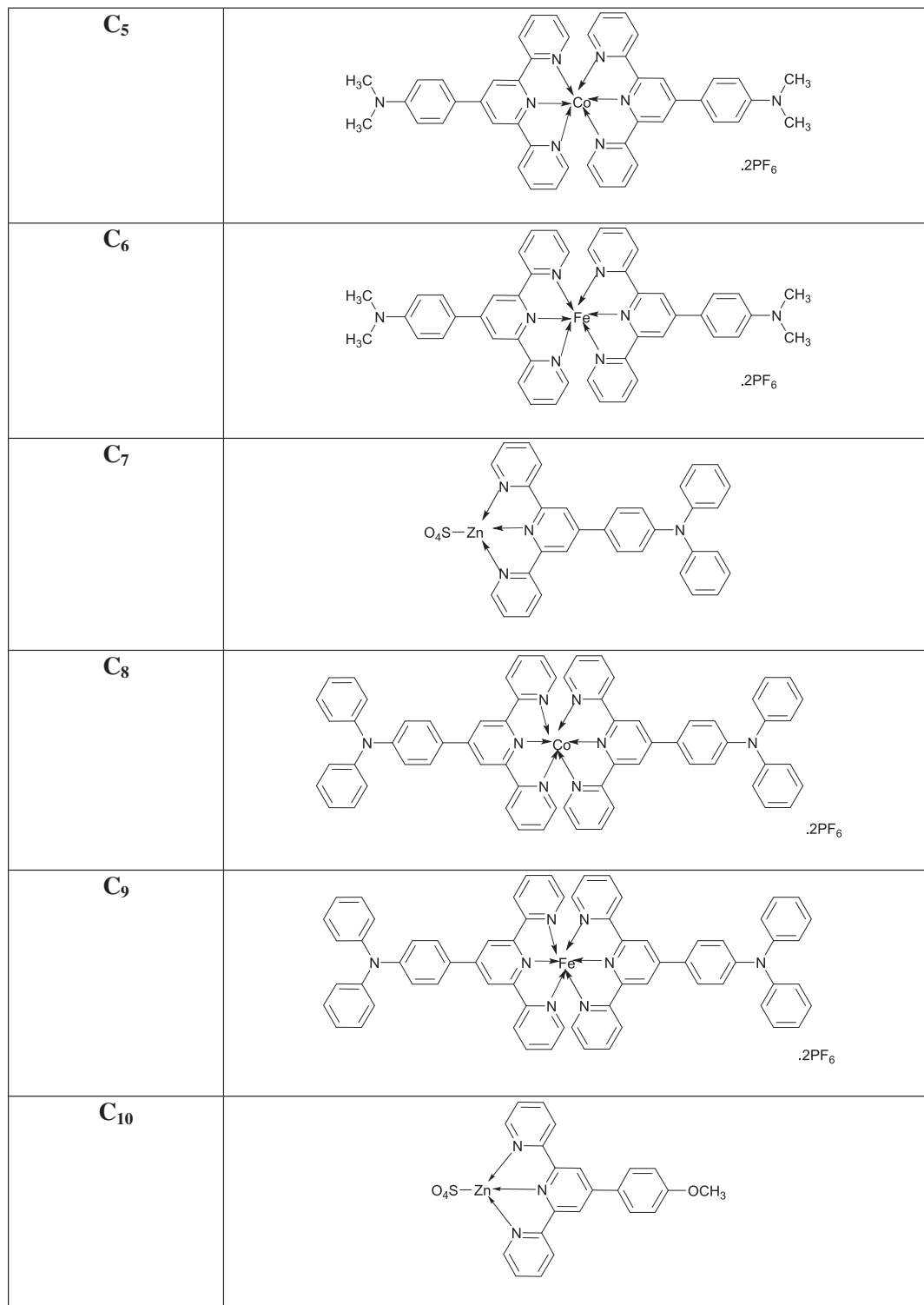
compound no.	structures
L₁	
L₂	
L₃	
L₄	
L₅	
L₆	

Scheme 1. (Continued.)

2H, Ar-H), 7.83 (ddd, $J = 3.0, 6.0, 9.0$ Hz, 2H, Ar-H), 7.67 (d, $J = 9.0$ Hz, 2H, Ar-H), 7.30–7.26 (m, 2H, Ar-H); ^{13}C NMR (75 MHz, CDCl_3) δ 156.3, 156.1, 149.0, 142.0, 139.0, 137.1, 127.3, 126.0, 126.0, 124.2, 124.0, 123.2, 121.4, 119.5, 119.1, 77.4, other carbons are isochronous.

L₇	
L₈	
L₉	
C₁	
C₂	
C₃	
C₄	

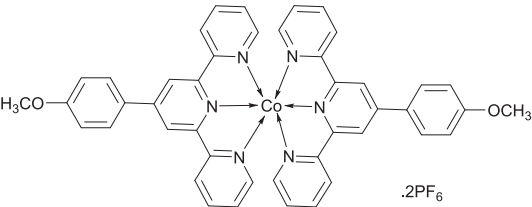
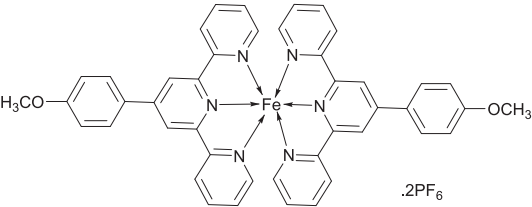
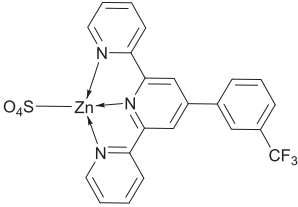
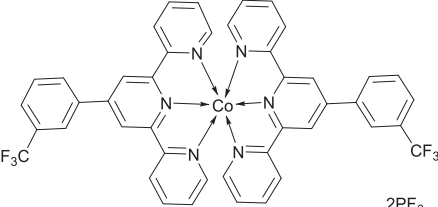
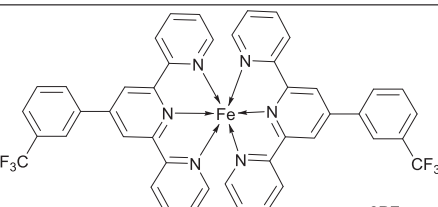
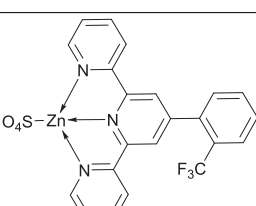
Scheme 1. (Continued.)



Scheme 1. (Continued.)

3.9. 4'-(3-Nitrophenyl)-2,2':6',2''-terpyridine (**L₈**) [82]

Brown amorphous solid; Yield 75%; m.p. 151–153°C; UV λ_{max} (CHCl₃) = 253 nm; λ_{em} (CHCl₃): 361, 723, 849 nm; FTIR (cm⁻¹): 3402 (C-H), 1613 (C=N), 1469 (C=C), 1346 (C-N), 834 (C-H), 787 (C-H); ¹H NMR (300 MHz, CDCl₃) δ 8.75 (d, *J* = 9.0 Hz, 1H, Ar-H), 8.69–8.65 (m, 4H, Ar-H), 8.62 (d, *J* = 9.0 Hz, 2H, Ar-H), 8.26–8.22 (m, 1H, Ar-H), 8.16–8.12 (m, 1H, Ar-H), 8.85–8.79 (m, 2H, Ar-H), 7.65–7.58 (m, 1H, Ar-H), 7.33–7.26 (m, 2H, Ar-H); ¹³C NMR (75 MHz, CDCl₃) δ 156.4, 156.1, 155.9,

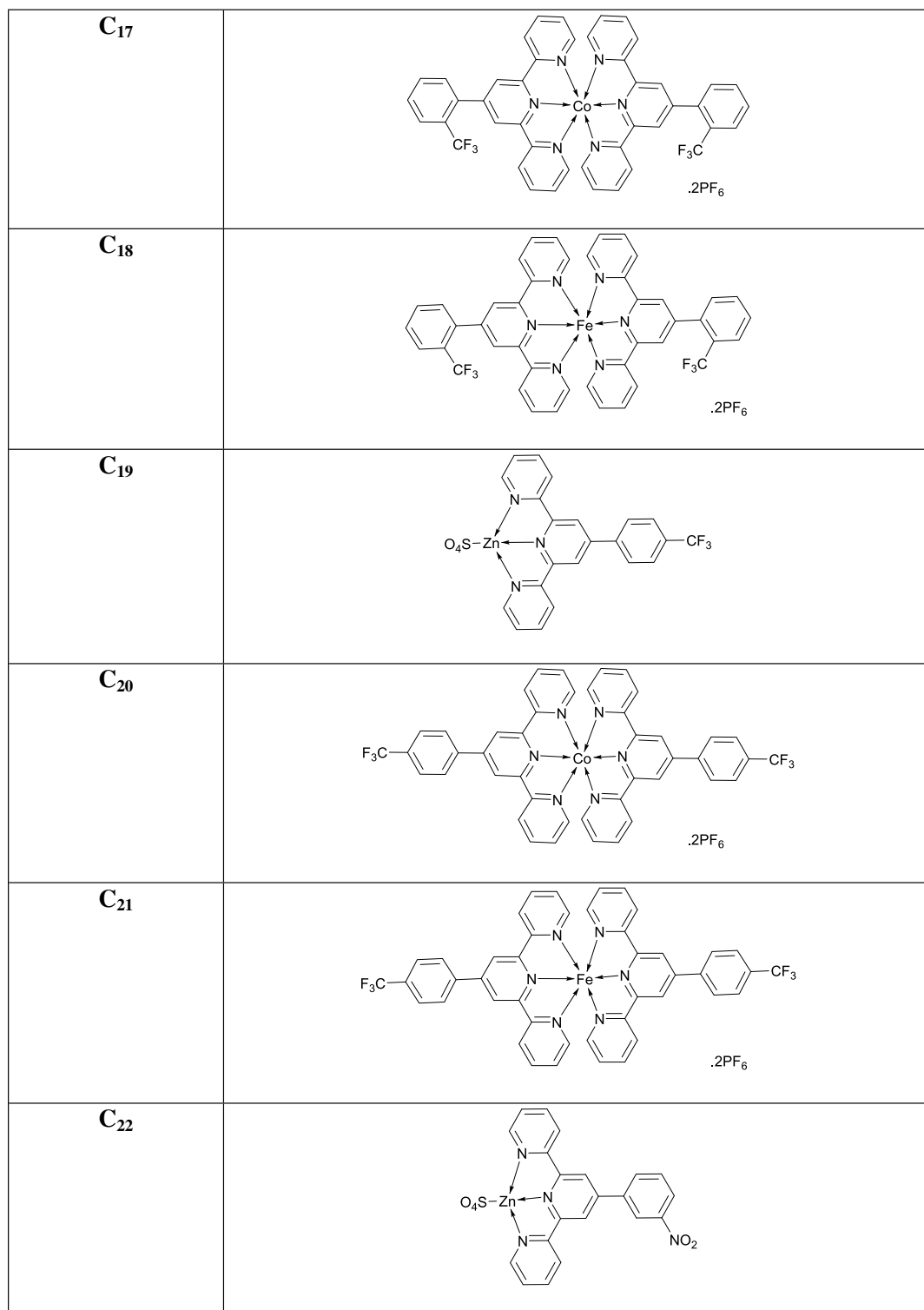
C₁₁	
C₁₂	
C₁₃	
C₁₄	
C₁₅	
C₁₆	

Scheme 1. (Continued.)

154.9, 148.9, 147.3, 140.5, 136.9, 133.2, 129.9, 125.3, 124.0, 123.9, 123.8, 123.0, 122.8, 122.3, 121.8, 120.7, 119.1, 118.6.

3.10. 4'-(4-Nitrophenyl)-2,2':6',2''-terpyridine (**L₉**)

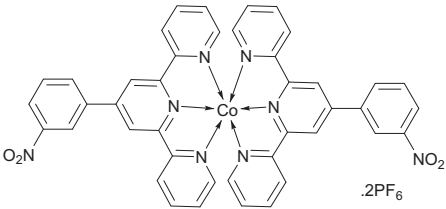
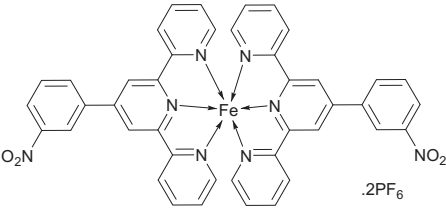
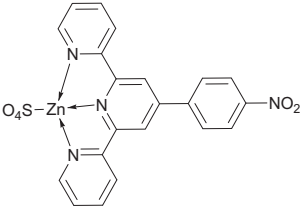
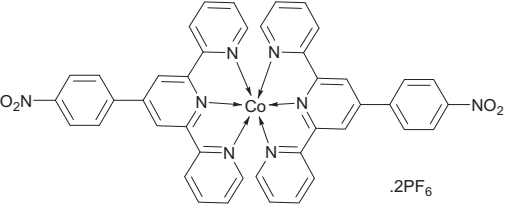
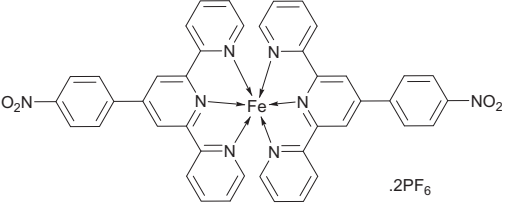
Reddish-brown amorphous solid; Yield 70%; m.p. 149–151°C; UV λ_{max} (CHCl₃) = 247 nm; λ_{em} (CHCl₃): 403, 720, 851 nm; FTIR (cm⁻¹): 3042 (C-H), 1582 (C=N), 1514 (C=C), 1265 (C-N), 1127 (C-H); ¹H NMR (300 MHz, CDCl₃) δ 8.74–8.68 (m, 4H, Ar-H), 8.65–8.60 (m, 2H, Ar-H), 8.25 (d, J = 9.0 Hz, 2H, Ar-H),

**Scheme 1.** (Continued.)

8.05 (ddd, $J = 3.0, 6.0, 9.0$ Hz, 2H, Ar-H), 7.97 (d, $J = 9.0$ Hz, 2H, Ar-H), 7.34–7.28 (m, 2H, Ar-H); ¹³C NMR (75 MHz, CDCl₃) δ 156.7, 156.5, 150.1, 143.1, 140.8, 137.5, 128.0, 125.8, 125.1, 124.5, 124.7, 123.6, 122.1, 120.0, 119.2, other carbons are isochronous.

3.11. [Zn(4'-(4-methylphenyl)-2,2':6',2''-terpyridine)(SO₄)] (C₁)

Light-purple amorphous solid; Yield: 85%; m.p. above 300°C; UV λ_{max} (CH₃CN) = 338 nm; λ_{em} (CH₃CN): 405, 704 nm; FTIR (cm⁻¹): 1617 (C=N), 1478 (C=C), 1249 (C-N), 1112 (C-H), 587 (Zn-N); MS (MALDI-ToF) of [M]⁺: 387.0713.

C₂₃	
C₂₄	
C₂₅	
C₂₆	
C₂₇	

Scheme 1. (Continued.)

3.12. [Co(4'-(4-methylphenyl)-2,2':6',2''-terpyridin)]₂(PF₆)₂ (**C₂**)

Brick-red amorphous solid; Yield: 85%; m.p. above 300°C; UV λ_{\max} (CH₃CN) = 314 nm; λ_{em} (CH₃CN): 379, 776 nm; FTIR (cm⁻¹): 1616 (C=N), 1471 (C=C), 1245 (C-N), 1110 (C-H), 623 (Co-N); MS (MALDI-ToF) of [M]⁺ : 705.2176.

3.13. [Fe(4'-(4-methylphenyl)-2,2':6',2''-terpyridin)]₂(PF₆)₂ (**C₃**)

Dark-purple amorphous solid; Yield: 79%; m.p. above 300°C; UV λ_{\max} (CH₃CN) = 327 nm; λ_{em} (CH₃CN): 394, 742 nm; FTIR (cm⁻¹): 1611 (C=N), 1483 (C=C), 1286 (C-N), 1058 (C-H), 627 (Fe-N); MS (MALDI-ToF) of [M]⁺ : 702.2194.

3.14. [Zn(N,N-dimethyl-4-(2,2':6',2''-terpyridin-4'-yl)aniline)](SO₄) (**C₄**)

Brown amorphous solid; Yield: 72%; m.p. above 300°C; UV λ_{\max} (CH₃CN) = 243 nm; λ_{em} (CH₃CN): 370, 521, 732 nm; FTIR (cm⁻¹): 1595 (C=N), 1476 (C=C), 1250 (C-N), 1107 (C-H), 584 (Zn-N); MS (MALDI-ToF) of [M]⁺ : 416.0979.

3.15. [Co(4'-(N,N-dimethyl-4-(2,2':6',2''-terpyridin-4'-yl)aniline)₂)](PF₆)₂ (**C₅**)

Candy-orange amorphous solid; Yield: 76%; m.p. above 300°C; UV λ_{\max} (CH₃CN) = 290 nm; λ_{em} (CH₃CN): 547, 683 nm; FTIR (cm⁻¹): 1595 (C=N), 1473 (C=C), 1248 (C-N), 1125 (C-H), 625 (Co-N); MS (MALDI-ToF) of [M]⁺ : 763.2707.

3.16. [Fe(4'-(N,N-dimethyl-4-(2,2':6',2''-terpyridin-4'-yl)aniline)₂)](PF₆)₂ (**C₆**)

Dark-purple amorphous solid; Yield: 77%; m.p. above 300°C; UV λ_{\max} (CH₃CN) = 324 nm; λ_{em} (CH₃CN): 365, 638, 751 nm; FTIR (cm⁻¹): 1587 (C=N), 1468 (C=C), 1247 (C-N), 1090 (C-H), 629 (Fe-N); MS (MALDI-ToF) of [M]⁺ : 760.2725.

3.17. [Zn(N,N-diphenyl-4-(2,2':6',2''-terpyridin-4'-yl)aniline)(SO₄)] (**C₇**)

Brown amorphous solid; Yield: 80%; m.p. above 300°C; UV λ_{\max} (CH₃CN) = 428 nm; λ_{em} (CH₃CN): 294, 359, 451, 717 nm; FTIR (cm⁻¹): 1660 (C=N), 1487 (C=C), 1286 (C-N), 1105 (C-H), 589 (Zn-N); MS (MALDI-ToF) of [M]⁺ : 540.1292.

3.18. [Co(N,N-diphenyl-4-(2,2':6',2''-terpyridin-4'-yl)aniline)₂](PF₆)₂ (**C₈**)

Marmalade (dark-yellow) amorphous solid; Yield: 70%; m.p. above 300°C; UV λ_{\max} (CH₃CN) = 308 nm; λ_{em} (CH₃CN): 273, 453, 722 nm; FTIR (cm⁻¹): 1584 (C=N), 1506 (C=C), 1284 (C-N), 1050 (C-H), 621 (Co-N); MS (MALDI-ToF) of [M]⁺ : 1011.3310.

3.19. [Fe(N,N-diphenyl-4-(2,2':6',2''-terpyridin-4'-yl)aniline)₂](PF₆)₂ (**C₉**)

Maroon amorphous solid; Yield: 66%; m.p. above 300°C; UV λ_{\max} (CH₃CN) = 437 nm; λ_{em} (CH₃CN): 341, 747 nm; FTIR (cm⁻¹): 1582 (C=N), 1505 (C=C), 1285 (C-N), 1150 (C-H), 627 (Fe-N); MS (MALDI-ToF) of [M]⁺ : 1008.3351.

3.20. [Zn(4'-(4-methoxyphenyl)-2,2':6',2''-terpyridine)(SO₄)] (**C₁₀**)

Greyish-purple amorphous solid; Yield: 78%; m.p. above 300°C; UV λ_{\max} (CH₃CN) = 286 nm; λ_{em} (CH₃CN): 454, 856 nm; FTIR (cm⁻¹): 1600 (C=N), 1477 (C=C), 1295 (C-N), 1110 (C-H), 581 (Zn-N); MS (MALDI-ToF) of [M]⁺ : 403.0663.

3.21. [Co(4'-(4-methoxyphenyl)-2,2':6',2''-terpyridine)₂](PF₆)₂ (**C₁₁**)

Clay-brown amorphous solid; Yield: 66%; m.p. above 300°C; UV λ_{\max} (CH₃CN) = 286 nm; λ_{em} (CH₃CN): 426, 704, 856 nm; FTIR (cm⁻¹): 1610 (C=N), 1473 (C=C), 1301 (C-N), 1098 (C-H), 625 (Co-N); MS (MALDI-ToF) of [M]⁺ : 737.2075.

3.22. [Fe(4'-(4-methoxyphenyl)-2,2':6',2''-terpyridine)₂](PF₆)₂ (**C₁₂**)

Dark-purple amorphous solid; Mol. Wt.: 1024.55 g mol⁻¹; Yield: 58%; m.p. above 300°C; UV λ_{\max} (CH₃CN) = 336 nm; λ_{em} (CH₃CN): 409, 503, 759, 854 nm; FTIR (cm⁻¹): 3345 (C=N), 1607 (C=C), 1432 (C-N), 1057 (C-H), 628 (Fe-N); MS (MALDI-ToF) of [M]⁺ : 734.2092.

3.23. [Zn(4'-[3-(trifluoromethyl)phenyl]-2,2':6',2''-terpyridine)(SO₄)] (**C₁₃**)

Red-violet amorphous solid; Yield: 73%; m.p. above 300°C; UV λ_{\max} (CH₃CN) = 287 nm; λ_{em} (CH₃CN): 853 nm; FTIR (cm⁻¹): 1616 (C=N), 1443 (C=C), 1326 (C-N), 1298 (C-H), 583 (Zn-N); MS (MALDI-ToF) of [M]⁺ : 441.0431.

3.24. [Co(4'-[3-(trifluoromethyl)phenyl]-2,2':6',2''-terpyridine)₂](PF₆)₂ (**C₁₄**)

Brick-red amorphous solid; Yield: 55%; m.p. above 300°C; UV λ_{\max} (CH₃CN) = 285 nm; λ_{em} (CH₃CN): 405, 737, 850 nm; FTIR (cm⁻¹): 1617 (C=N), 1473 (C=C), 1327 (C-N), 1250 (C-H) 627 (Co-N); MS (MALDI-ToF) of [M]⁺: 813.1611.

3.25. [Fe(4'-[3-(trifluoromethyl)phenyl]-2,2':6',2''-terpyridine)₂](PF₆)₂ (**C₁₅**)

Dark-purple amorphous solid; Yield: 70%; m.p. above 300°C; UV λ_{\max} (CH₃CN) = 286 nm; λ_{em} (CH₃CN): 403, 685, 850 nm; FTIR (cm⁻¹): 1612 (C=N), 1448 (C=C), 1327 (C-N), 1128 (C-H), 630 (Fe-N); MS (MALDI-ToF) of [M]⁺: 810.1629.

3.26. [Zn(4'-[2-(trifluoromethyl)phenyl]-2,2':6',2''-terpyridine)(SO₄)] (**C₁₆**)

Lilac (light purple) amorphous solid; Yield: 65%; m.p. above 300°C; UV λ_{\max} (CH₃CN) = 283 nm; λ_{em} (CH₃CN): 401, 685, 851 nm; FTIR (cm⁻¹): 1617 (C=N), 1447 (C=C), 1327 (C-N), 1284 (C-H), 590 (Zn-N); MS (MALDI-ToF) of [M]⁺: 441.0431.

3.27. [Co(4'-[2-(trifluoromethyl)phenyl]-2,2':6',2''-terpyridine)₂](PF₆)₂ (**C₁₇**)

Brick-red amorphous solid; Yield: 78%; m.p. above 300°C; UV λ_{\max} (CH₃CN) = 285 nm; λ_{em} (CH₃CN): 361, 735, 859 nm; FTIR (cm⁻¹): 1615 (C=N), 1476 (C=C), 1328 (C-N), 1197 (C-H), 627 (Co-N); MS (MALDI-ToF) of [M]⁺: 813.1611.

3.28. [Fe(4'-[2-(trifluoromethyl)phenyl]-2,2':6',2''-terpyridine)₂](PF₆)₂ (**C₁₈**)

Dark-purple amorphous solid; Yield: 71%; m.p. above 300°C; UV λ_{\max} (CH₃CN) = 286 nm; λ_{em} (CH₃CN): 361, 580, 737, 865 nm; FTIR (cm⁻¹): 1612 (C=N), 1450 (C=C), 1328 (C-N), 1265 (C-H), 629 (Fe-N); MS (MALDI-ToF) of [M]⁺: 810.1629.

3.29. [Zn(4'-[4-(trifluoromethyl)phenyl]-2,2':6',2''-terpyridine)(SO₄)] (**C₁₉**)

Light-purple amorphous solid; Yield: 70%; m.p. above 300°C; UV λ_{\max} (CH₃CN) = 286 nm; λ_{em} (CH₃CN): 409, 856 nm; FTIR (cm⁻¹): 1619 (C=N), 1448 (C=C), 1329 (C-N), 1198 (C-H), 592 (Zn-N); MS (MALDI-ToF) of [M]⁺: 441.0431.

3.30. [Co(4'-[4-(trifluoromethyl)phenyl]-2,2':6',2''-terpyridine)₂](PF₆)₂ (**C₂₀**)

Chocolate-brown amorphous solid; Yield: 65%; m.p. above 300°C; UV λ_{\max} (CH₃CN) = 289 nm; λ_{em} (CH₃CN): 360, 730, 867 nm; FTIR (cm⁻¹): 1617 (C=N), 1480 (C=C), 1332 (C-N), 1267 (C-H), 623 (Co-N); MS (MALDI-ToF) of [M]⁺: 813.1611.

3.31. [Fe(4'-[4-(trifluoromethyl)phenyl]-2,2':6',2''-terpyridine)₂](PF₆)₂ (**C₂₁**)

Dark-purple amorphous solid; Yield: 66%; m.p. above 300°C; UV λ_{\max} (CH₃CN) = 286 nm; λ_{em} (CH₃CN): 358, 578, 732, 869 nm; FTIR (cm⁻¹): 1615 (C=N), 1457 (C=C), 1334 (C-N), 1210 (C-H), 626 (Fe-N); MS (MALDI-ToF) of [M]⁺: 810.1629.

3.32. [Zn(4'-(3-nitrophenyl)-2,2':6',2''-terpyridine)(SO₄)] (**C₂₂**)

Light-purple amorphous solid; Yield: 74%; m.p. above 300°C; UV λ_{\max} (CH₃CN) = 347 nm; λ_{em} (CH₃CN): 365, 680, 743, 855; FTIR (cm⁻¹): 1603 (C=N), 1467 (C=C), 1348 (C-N), 1073 (C-H), 585 (Zn-N); MS (MALDI-ToF) of [M]⁺: 310.040.

3.33. [Co(4'-(3-nitrophenyl)-2,2':6',2''-terpyridine)₂](PF₆)₂ (C₂₃)

Chocolate-brown amorphous solid; Yield: 65%; m.p. above 300°C; UV λ_{\max} (CH₃CN) = 334 nm; λ_{em} (CH₃CN): 391, 699 nm; FTIR (cm⁻¹): 1614 (C=N), 1530 (C=C), 1246 (C-N), 1151 (C-H), 627 (Co-N); MS (MALDI-ToF) of [M]⁺ : 767.1565.

3.34. [Fe(4'-(3-nitrophenyl)-2,2':6',2''-terpyridine)₂](PF₆)₂ (C₂₄)

Dark-purple amorphous solid; Yield: 70%; m.p. above 300°C; UV λ_{\max} (CH₃CN) = 328 nm; λ_{em} (CH₃CN): 402, 684, 856 nm; FTIR (cm⁻¹): 1614 (C=N), 1474 (C=C), 1351 (C-N), 1025 (C-H), 629 (Fe-N); MS (MALDI-ToF) of [M]⁺ : 764.1584.

3.35. [Zn(4'-(4-nitrophenyl)-2,2':6',2''-terpyridine)(SO₄)] (C₂₅)

Caramel (brown) amorphous solid; Yield: 77%; m.p. above 300°C; UV λ_{\max} (CH₃CN) = 287 nm; λ_{em} (CH₃CN): 474, 850 nm; FTIR (cm⁻¹): 1619 (C=N), 1476 (C=C), 1359 (C-N), 1167 (C-H), 587 (Zn-N); MS (MALDI-ToF) of [M]⁺ : 310.040.

3.36. [Co(4'-(4-nitrophenyl)-2,2':6',2''-terpyridine)₂](PF₆)₂ (C₂₆)

Chocolate-brown amorphous solid; Yield: 76%; m.p. above 300°C; UV λ_{\max} (CH₃CN) = 289 nm; λ_{em} (CH₃CN): 428, 563, 850 nm; FTIR (cm⁻¹): 1616 (C=N), 1471 (C=C), 1245 (C-N), 1245 (C-H), 628 (Co-N); MS (MALDI-ToF) of [M]⁺ : 767.1565.

3.37. [Fe(4'-(4-nitrophenyl)-2,2':6',2''-terpyridine)₂](PF₆)₂ (C₂₇)

Dark-purple amorphous solid; Yield: 83%; m.p. above 300°C; UV λ_{\max} (CH₃CN) = 287 nm; λ_{em} (CH₃CN): 565, 848 nm; FTIR (cm⁻¹): 1618 (C=N), 1472 (C=C), 1350 (C-N), 1287 (C-H), 630 (Fe-N); MS (MALDI-ToF) of [M]⁺ : 764.1598.

3.38. Absorption properties

With a broad class of terpyridine compounds in hand, we examined their initial photophysical properties. The UV-Vis spectra of terpyridines and their metal complexes are recorded in chloroform and acetonitrile solutions, respectively, and the related data are given in table 1. In the absorption spectra recorded in chloroform for the ligands (L₁–L₉), strong, broad absorption bands appear in the range 234–325 nm, while for the complexes (C₁–C₂₇), the absorption bands were seen in the range 240–429 nm. All these absorptions are attributed to π – π^* electronic transitions in the aromatic system of the terpyridines. The absorption maxima for C₁–C₂₇ are somewhat shifted from those of the free ligands by affixing either electron-releasing or -withdrawing groups at the central pyridine. The longest absorption wavelength in the L₁ UV-Vis spectrum (λ_{\max} = 325 nm) is broad and comparable to that of the un-substituted parent terpyridine (table 1). The UV-Vis spectra of the Zn(II), Co(II) and Fe(II) complexes in acetonitrile solutions are shown in electronic supplementary material, table S1. The variation in absorption wavelengths and intensities is the result of different substituents in the 4' position of the terpyridine. The UV-Vis spectra of terpyridine-based metal complexes show the characteristic metal–ligand charge transfer (MLCT) shift of the Fe(II)-terpyridine system (C₃, C₆, C₉, C₁₂, C₁₅, C₁₈, C₂₁, C₂₄, C₂₇) at λ_{\max} = 587 nm and the bands at 284 nm and 426 nm are due to ligand-centred (LC) transitions. A slight redshift when related to the reference iron (II) terpyridine complex has been detected. The spin allowed the MLCT band in the visible region to undergo a rise in intensity and a redshift, regardless of electron-donor or -acceptor nature of the substituents. The intense absorption bands of the Zn(II) complexes (C₁, C₄, C₇, C₁₀, C₁₃, C₁₆, C₁₉, C₂₂, C₂₅) were seen in the range 215–586 nm. These absorption peaks are mainly due to the metal–ligand charge transfer of π – π^* and n – π^* transitions having λ_{\max} = 586 nm. This redshift could be credited to a decrease in the LUMO energy values of the complexes. The absorption bands of the Co(II) complexes (C₂, C₅, C₈, C₁₁, C₁₄, C₁₇, C₂₀, C₂₃, C₂₆) were seen in the range 209–571 nm and their MLCT transitions have a maximum value at 530 nm.

Surprisingly, the electron-donating group *p*-methoxyphenyl at the 4'-position of the terpyridine ring in Zn(II) and Co(II) complexes shifts λ_{\max} towards longer wavelengths, resulting in a 30 nm bathochromic

Table 1. Absorption and emission data of all the synthesized compounds.

compound code	solvent	excitation wavelength (nm)	λ_{em} (nm)	λ_{max} (nm)	transitions	MLCT band	Stokes shift (nm)
L ₁	chloroform	335	357, 731	325	$\pi-\pi^*$ (LC)	—	374
L ₂	chloroform	303	344, 443	293	$\pi-\pi^*$ (LC)	—	109
L ₃	chloroform	243	335, 576	234	$\pi-\pi^*$ (LC)	—	241
L ₄	chloroform	258	371, 746, 855	248	$\pi-\pi^*$ (LC)	—	109
L ₅	chloroform	243	359, 727, 861	234	$\pi-\pi^*$ (LC)	—	134
L ₆	chloroform	250	345, 70, 85	240	$\pi-\pi^*$ (LC)	—	15
L ₇	chloroform	243	345, 723, 852	234	$\pi-\pi^*$ (LC)	—	129
L ₈	chloroform	263	361, 723, 849	253	$\pi-\pi^*$ (LC)	—	126
L ₉	chloroform	257	403, 720, 851	247	$\pi-\pi^*$ (LC)	—	131
C ₁	acetonitrile	348	405, 704	338	$\pi-\pi^*$ (C=C), $n-\pi^*$ (C=N)	575 (d $\pi \rightarrow \pi^*$)	299
C ₂	acetonitrile	324	379, 776	314	$\pi-\pi^*$ (C=C), $n-\pi^*$ (C=N)	523 (d $\pi \rightarrow \pi^*$)	397
C ₃	acetonitrile	337	394, 742	327	$\pi-\pi^*$ (C=C), $n-\pi^*$ (C=N)	571 (d $\pi \rightarrow \pi^*$)	348
C ₄	acetonitrile	253	370, 521, 732	243	$\pi-\pi^*$ (C=C), $n-\pi^*$ (C=N)	580 (d $\pi \rightarrow \pi^*$)	211
C ₅	acetonitrile	300	547, 683	290	$\pi-\pi^*$ (C=C), $n-\pi^*$ (C=N)	442 (d $\pi \rightarrow \pi^*$)	136
C ₆	acetonitrile	334	365, 638, 751	324	$\pi-\pi^*$ (C=C), $n-\pi^*$ (C=N)	587 (d $\pi \rightarrow \pi^*$)	113
C ₇	acetonitrile	438	294, 359, 451, 717	428	$\pi-\pi^*$ (C=C), $n-\pi^*$ (C=N)	583 (d $\pi \rightarrow \pi^*$)	266
C ₈	acetonitrile	318	273, 453, 722	308	$\pi-\pi^*$ (C=C), $n-\pi^*$ (C=N)	447 (d $\pi \rightarrow \pi^*$)	269
C ₉	acetonitrile	447	341, 747	437	$\pi-\pi^*$ (C=C), $n-\pi^*$ (C=N)	584 (d $\pi \rightarrow \pi^*$)	406
C ₁₀	acetonitrile	296	454, 856	286	$\pi-\pi^*$ (C=C), $n-\pi^*$ (C=N)	586 (d $\pi \rightarrow \pi^*$)	402
C ₁₁	acetonitrile	296	426, 704, 856	286	$\pi-\pi^*$ (C=C), $n-\pi^*$ (C=N)	538 (d $\pi \rightarrow \pi^*$)	152
C ₁₂	acetonitrile	346	409, 503, 759, 854	336	$\pi-\pi^*$ (C=C), $n-\pi^*$ (C=N)	586 (d $\pi \rightarrow \pi^*$)	95
C ₁₃	acetonitrile	297	853	287	$\pi-\pi^*$ (C=C), $n-\pi^*$ (C=N)	570 (d $\pi \rightarrow \pi^*$)	568
C ₁₄	acetonitrile	295	405, 737, 850	285	$\pi-\pi^*$ (C=C), $n-\pi^*$ (C=N)	526 (d $\pi \rightarrow \pi^*$)	113

(Continued.)

Table 1. (Continued.)

compound code	solvent	excitation wavelength (nm)	λ_{em} (nm)	λ_{max} (nm)	transitions	MLCT band	Stokes shift (nm)
C ₁₅	acetonitrile	296	403, 685, 850	286	$\pi-\pi^*$ ($C=C$), $n-\pi^*$ ($C=N$)	568 ($d\pi \rightarrow \pi^*$)	165
C ₁₆	acetonitrile	293	401, 685, 851	283	$\pi-\pi^*$ ($C=C$), $n-\pi^*$ ($C=N$)	569 ($d\pi \rightarrow \pi^*$)	166
C ₁₇	acetonitrile	295	361, 735, 859	285	$\pi-\pi^*$ ($C=C$), $n-\pi^*$ ($C=N$)	538 ($d\pi \rightarrow \pi^*$)	124
C ₁₈	acetonitrile	296	361, 580, 737, 865	286	$\pi-\pi^*$ ($C=C$), $n-\pi^*$ ($C=N$)	572 ($d\pi \rightarrow \pi^*$)	128
C ₁₉	acetonitrile	296	409, 856	286	$\pi-\pi^*$ ($C=C$), $n-\pi^*$ ($C=N$)	540 ($d\pi \rightarrow \pi^*$)	447
C ₂₀	acetonitrile	299	360, 730, 867	289	$\pi-\pi^*$ ($C=C$), $n-\pi^*$ ($C=N$)	435 ($d\pi \rightarrow \pi^*$)	137
C ₂₁	acetonitrile	296	358, 578, 733, 869	286	$\pi-\pi^*$ ($C=C$), $n-\pi^*$ ($C=N$)	569 ($d\pi \rightarrow \pi^*$)	138
C ₂₂	acetonitrile	357	365, 680, 743, 855	347	$\pi-\pi^*$ ($C=C$), $n-\pi^*$ ($C=N$)	580 ($d\pi \rightarrow \pi^*$)	112
C ₂₃	acetonitrile	344	391, 699	334	$\pi-\pi^*$ ($C=C$), $n-\pi^*$ ($C=N$)	535 ($d\pi \rightarrow \pi^*$)	308
C ₂₄	acetonitrile	338	402, 684, 856	328	$\pi-\pi^*$ ($C=C$), $n-\pi^*$ ($C=N$)	575 ($d\pi \rightarrow \pi^*$)	172
C ₂₅	acetonitrile	297	474, 850	287	$\pi-\pi^*$ ($C=C$), $n-\pi^*$ ($C=N$)	581 ($d\pi \rightarrow \pi^*$)	376
C ₂₆	acetonitrile	299	428, 563, 850	289	$\pi-\pi^*$ ($C=C$), $n-\pi^*$ ($C=N$)	545 ($d\pi \rightarrow \pi^*$)	287
C ₂₇	acetonitrile	297	565, 848	287	$\pi-\pi^*$ ($C=C$), $n-\pi^*$ ($C=N$)	583 ($d\pi \rightarrow \pi^*$)	283

LC = ligand centred transition.

MLCT = metal to ligand charge transfer transition.

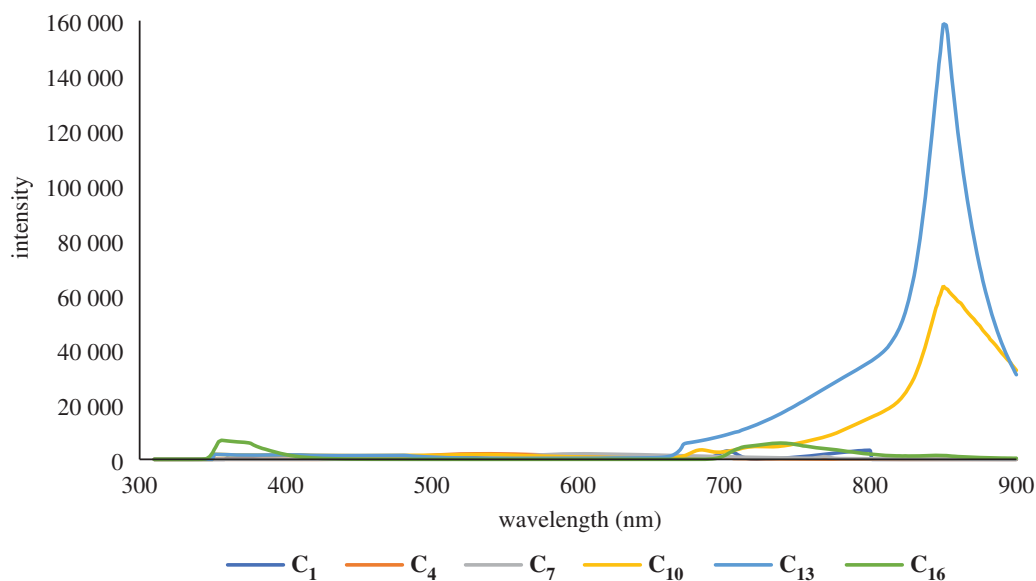


Figure 2. A comparison of emission spectra of Zn complexes of L_1-L_6 in solution form.

shift. This result supports the concept that the MLCT state can be higher in energy by nitration of the terpyridine ligand-based metal complexes, the 4-methoxyphenyl group at the 4'-position of the terpyridine ring in the complexes have a shorter wavelength, and a significant maximum enhancement in MLCT band energy was observed. The absorption bands are influenced significantly by the aryl substituents on the terminal phenyl moiety. Generally, the absorption spectra of all complexes are typically well correlated with those found for the respective uncomplexed ligands.

3.39. Photo-luminescent properties

Attaching various functional groups to terpyridine at the *p*-position may not only open several paths towards the development of advanced supramolecular structures but may also influence the fluorescence properties of the compounds. Due to their potential applications in chemical sensors, electroluminescent displays and fluorescent materials, inorganic-organic hybrid complexes, particularly those with d^{10} transition metal centres, are now of great interest. From the structural analysis, the ligand can be seen to have a large *p*-conjugated aromatic system that can possess strong fluorescence and efficient transfer of energy. The photo-luminescence spectra of the Zn, Co and Fe (C_1-C_{27}) complexes were recorded in acetonitrile solutions at ambient temperature with an excitation λ of 320 nm for the Zn(II) complexes, 286 nm for the Co complexes and 295 nm for the Fe complexes. All C_1-C_{27} complexes display emission bands in the visible region of the electromagnetic spectrum. The maximum emission peaks for the Zn, Co and Fe complexes were observed at 857, 859 and 865 nm, respectively, as described in table 1. The compounds having the lowest energy-absorption bands, which are below 310 nm, are not much different from the parent compounds. Fluorescence of L_1-L_9 was observed at about 340 nm irrespective of the location of the substitution and the number of phenyl groups. The excitation spectrum observed between 330 and 400 nm at any stage was similar to the corresponding absorption spectra, indicating that the excitation of the lowest energy absorption of L_1-L_9 led to the emitting state. In the *p*-position of the 4-phenyl complex, several substituents with different electron-donating or -withdrawing properties were added to further analyse and modify the fluorescence properties of 4-phenyl terpyridine. The *p*-substituted terpyridine complexes C_1-C_{27} absorption and fluorescence maxima are listed in table 1.

The photo-luminescent properties of compounds C_1-C_4 in solution and at ambient temperature are characterized by the fluorescence spectra presented in figures 2–4 and supporting information file. Compound C_1 has two bands in its emission spectrum, a lower intensity one at *ca* 405 nm and another with higher intensity at *ca* 704 nm. Similarly, compound C_2 has two bands in its emission spectra, a low-intensity one at *ca* 379 nm and another with higher intensity at *ca* 776 nm. Compared with the previously reported [66] photo-luminescence of the ligand L_1 , the higher energy bands of L_1 and L_2 may tentatively be assigned to an intra-ligand charge transfer (ILCT), while the latter band of C_1 is assumed to be the ligand–metal charge transfer (LMCT) and that of C_2 to a ligand-based intramolecular

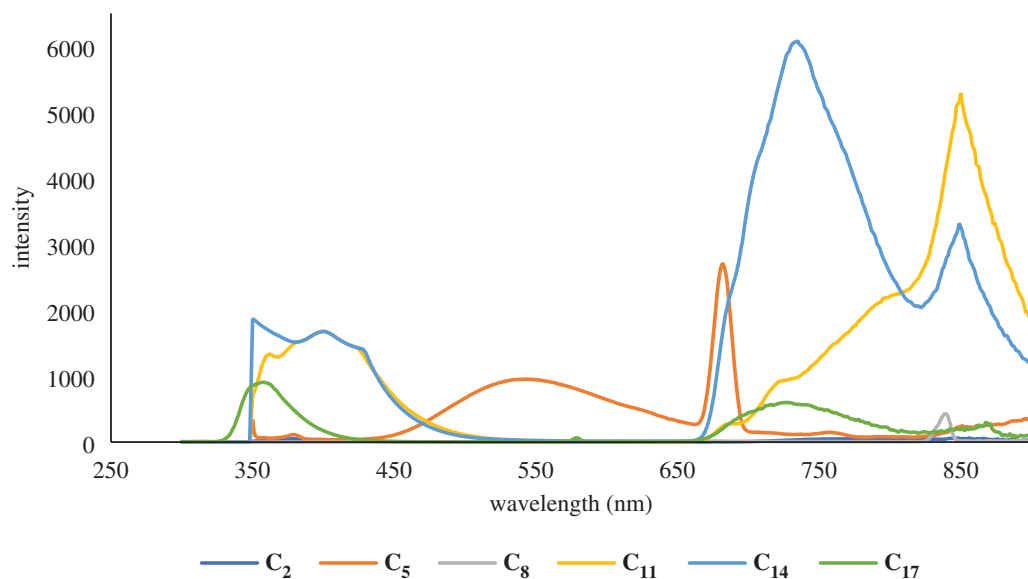


Figure 3. A comparison of emission spectra of Co complexes of L_1 – L_6 in solution form.

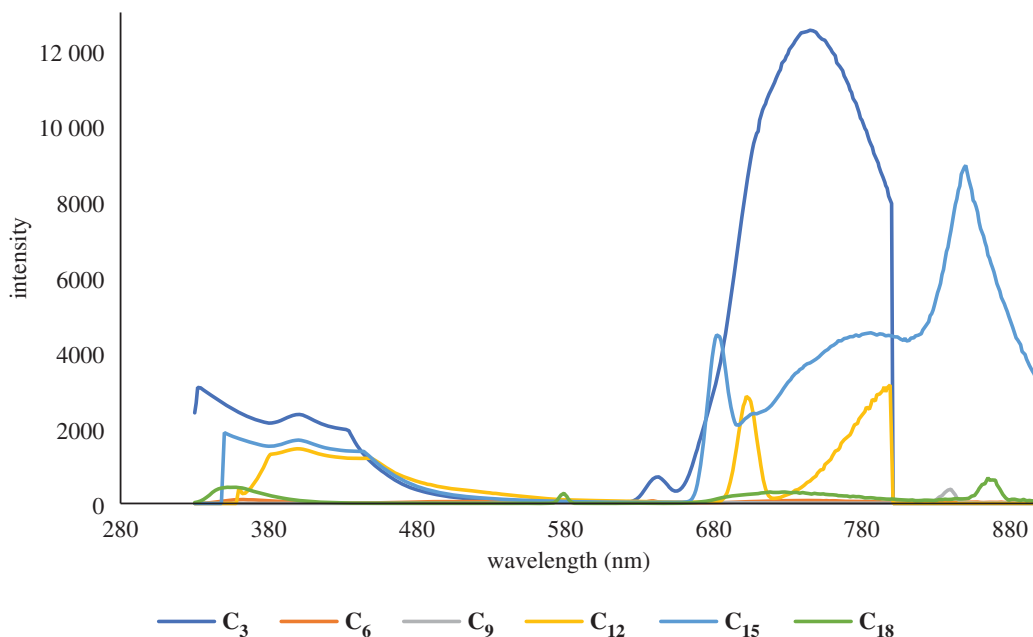


Figure 4. A comparison of emission spectra of Fe complexes of L_1 – L_6 in solution state.

charge transfer (ICT). In C_3 , the narrow band is present at 394 nm and broad band at 742 nm is also seen. This band is linked to an ILCT based on its energy that is similar to that recorded for a related $FeSO_4$ complex, which shows three bands, one at 402 nm, and the other two bands at 684 and 856 nm, respectively. The higher energy ILCT band (at 402 nm in C_3) is not sensitive to the transition from a 3d to a 4d metal complex (in the same group). The C_4 emission spectrum also displays three bands, one strong at 370 nm, one of low intensity at approximately 521 nm and a broad band at 732 nm. According to the results noted above, the former peak is tentatively assigned to an ILCT transition and the latter to an LMCT transition. From the structural analysis, it can be seen that ligand has a large π -conjugated aromatic system, which may possess strong fluorescence and efficient energy transfer. The free ligand L exhibits intense fluorescence with emission maxima at 372 and 522 nm upon excitation at 300 nm, while complexes show bright fluorescence with maximum emission at 547 and 683 nm for C_5 , 365 nm for C_6 and 359 nm for C_7 upon excitation at 312 nm. The emission values for complexes C_8 – C_{27} were in the range of 453 to 856 nm upon excitation at about 340 nm. The difference in emissions between the

ligands and the complexes is due to the various energy transfer routes, and the emissions detected in the complexes may be ascribed to the intra-ligand $\pi-\pi^*$ transitions.

The different substituents on terpyridine moiety in the Co(II) complexes generate a wider range for their emission spectra (365–850 nm) than for the Zn(II) and Fe(II) complexes. Substitution of relatively low electron-donating or withdrawal groups, such as methyl, only had a slight effect on the overall fluorescence properties.

3.40. Anti-microbial evaluation

Many microorganisms are becoming immune to traditional antibiotics and thus there is a need to introduce new antibiotics against those pathogens. In this regard, all the new compounds were assessed for their *in vitro* anti-bacterial activity against Gram-positive bacteria *Staphylococcus aureus* (ATCC 6538) and two Gram-negative bacteria *Escherichia coli* (ATCC 25922) and *Pseudomonas aeruginosa* (ATCC 9721). In addition, these compounds were evaluated for their anti-fungal activity against *Candida albicans* (ATCC 9002) and *Candida parapsilosis* (ATCC 22019) fungal strains. The results were recorded as the average diameter of ZOI of fungal or bacterial growth around the plates in millimetres for each compound tested. Both anti-bacterial and anti-fungal results are displayed in table 2.

3.41. Anti-bacterial activity

Anti-bacterial activity of the compounds has been checked against three bacterial strains including *P. aeruginosa*, *S. aureus*, *E. coli* using a well diffusion method. Henceforth, the relative screening of anti-bacterial activity of the new terpyridine-based ligands, L_1 to L_9 , and their metal complexes, C_1 to C_{27} , have been carried out on Gram-positive and Gram-negative bacteria. Cefixime was used as a standard. An assessment of anti-bacterial activity among all the compounds showed them to be very potent against *P. aeruginosa* and *E. coli*. The free ligand has considerable activity against *P. aeruginosa* and *E. coli* (ZOI ≥ 20 mm) but has moderate activity against *S. aureus* (ZOI ≤ 17 mm). In contrast with the free terpyridine ligand, the complex has more potent activity against *E. coli* (more ZOI), but it is less active against *S. aureus*. *In vitro*, anti-bacterial studies showed that all the complexes showed varying degrees of inhibition. Among the metal complexes, C_1 displayed excellent activity against *E. coli* with ZOI = 23.7 mm while C_8 , having ZOI = 20.7 mm, showed better activity compared with C_{22} and C_{23} having ZOI = 18.8 and 17.8 mm, respectively. In the case of *P. aeruginosa*, complexes C_{24} , C_8 and C_6 showed potential IZ diameters of 18.5, 17.3 and 17.2 mm respectively, as compared with complexes C_3 and C_1 . However, the compounds under examination were found to be almost inactive against *Staphylococcus aureus*, except C_1 , C_{22} and C_{24} , which showed ZOIs of about 16.5, 14.5 and 15.7 mm, respectively. Thus, all-metal complexes showed significant ZOIs against *P. Aeruginosa* and *E. coli* as compared with *S. aureus*. A comparative review of anti-bacterial findings indicated that the metal complexes displayed improved anti-bacterial activity compared with free ligands, as previously reported, from L_1 to L_9 . The remaining members of this series displayed moderate to good anti-bacterial activity and are comparatively more active against *P. aeruginosa* and *E. Coli* bacteria than *S. aureus* strain.

3.42. Anti-fungal activity

The new compounds were also evaluated against the two different fungal strains *C. albicans* and *C. parapsilosis*. The outcomes of these anti-fungal activities have been presented in table 2. The standard drug used was clotrimazole. Terpyridine analogues (L_1 – L_9) were found less active as compared with the standard. Again, the compounds C_{24} , C_{16} and C_8 , having ZOI values of 21.6, 19.8 and 19.5 mm, respectively, exhibited the highest activity against both fungal strains. However, these compounds were found comparatively more potent against fungi as compared with the bacteria. Although with respect to the standard drug, all the evaluated compounds were found to show moderate to good activity against both *C. albicans* and *C. parapsilosis* fungi.

3.43. Structure–activity and structure–property relationships

As far as absorption behaviour is concerned, the absorption bands are influenced significantly by the aryl substituents on the terminal aryl moiety. Compared with the phenyl-substituted compound, electron-

Table 2. Anti-microbial assay (ZOI) of all the synthesized compounds.

compound number	zones of inhibition (mm)				
	anti-bacterial activity			anti-fungal activity	
	<i>P. aeruginosa</i>	<i>S. aureus</i>	<i>E. coli</i>	<i>C. albicans</i>	<i>C. parapsilosis</i>
L ₁	0	0	14.5 ± 0.7	11.8 ± 0.7	0
L ₂	15.1 ± 0.7	0	16.5 ± 0.4	12 ± 0.1	0
L ₃	0	0	16.5 ± 0.1	0	0
L ₄	0	0	15.5 ± 0.2	19.3 ± 0.3	14.6 ± 0.1
L ₅	0	0	17.5 ± 0.3	17.3 ± 0.2	17.5 ± 0.7
L ₆	14.3 ± 0.3	0	0	17.4 ± 0.5	17.5 ± 0.4
L ₇	18.1 ± 0.4	0	0	15.3 ± 0.2	0
L ₈	0	0	0	0	14.7 ± 0.8
L ₉	0	0	18.7 ± 0.7	0	11.6 ± 0.6
C ₁	16.3 ± 0.7	16.5 ± 0.7	23.7 ± 0.5	17.3 ± 0.6	0
C ₂	16.5 ± 0.7	0	20.8 ± 0.5	18.9 ± 0.6	0
C ₃	16.7 ± 0.1	0	16.7 ± 0.6	11.4 ± 0.5	18.7 ± 0.3
C ₄	17.9 ± 0.3	18.5 ± 0.7	15.4 ± 0.3	0	0
C ₅	17.2 ± 0.3	13.5 ± 0.7	15.7 ± 0.3	0	14.7 ± 0.3
C ₆	17.2 ± 0.3	0	15.7 ± 0.3	0	0
C ₇	19.3 ± 0.1	12.5 ± 0.4	21.7 ± 0.4	0	14.6 ± 0.6
C ₈	17.3 ± 0.1	14.5 ± 0.4	20.7 ± 0.4	19.5 ± 0.7	15.6 ± 0.6
C ₉	0	0	0	0	12.6 ± 0.5
C ₁₀	17.3 ± 0.2	15.7 ± 0.5	14.8 ± 0.2	0	0
C ₁₁	14.2 ± 0.2	0	13.8 ± 0.3	18.8 ± 0.6	0
C ₁₂	11.5 ± 0.4	17.5 ± 0.4	0	12.6 ± 0.6	18.3 ± 0.7
C ₁₃	14.3 ± 0.3	15.7 ± 0.3	18.8 ± 0.5	0	15.8 ± 0.8
C ₁₄	18.2 ± 0.2	0	19.8 ± 0.3	13.8 ± 0.6	18.6 ± 0.9
C ₁₅	0	0	0	0	15.7 ± 0.7
C ₁₆	19.3 ± 0.3	16.8 ± 0.5	12.8 ± 0.5	19.8 ± 0.1	18.8 ± 0.6
C ₁₇	12.2 ± 0.2	0	0	15.8 ± 0.6	12.4 ± 0.5
C ₁₈	14.5 ± 0.4	0	0	0	15.3 ± 0.7
C ₁₉	18.3 ± 0.3	15.7 ± 0.3	18.8 ± 0.5	15.8 ± 0.1	0
C ₂₀	0	0	16.8 ± 0.3	0	14.6 ± 0.5
C ₂₁	18.5 ± 0.4	0	0	21.6 ± 0.6	0
C ₂₂	14.3 ± 0.3	15.7 ± 0.3	14.8 ± 0.5	15.8 ± 0.1	16.8 ± 0.6
C ₂₃	14.2 ± 0.2	0	19.8 ± 0.3	15.8 ± 0.6	10.6 ± 0.5
C ₂₄	18.5 ± 0.4	0	0	21.6 ± 0.6	15.3 ± 0.7
C ₂₅	19.3 ± 0.3	14.7 ± 0.3	17.8 ± 0.5	15.8 ± 0.1	12.8 ± 0.6
C ₂₆	16.2 ± 0.2	0	15.8 ± 0.3	18.8 ± 0.6	0
C ₂₇	17.5 ± 0.4	18.7 ± 0.3	0	0	11.3 ± 0.7
negative (DMSO)	—	—	—	—	—
standard (cefixime)	28.7 ± 0.3	27.5 ± 0.7	30.5 ± 0.3	—	—
standard (clotrimazole)	—	—	—	28.9 ± 0.8	25.6 ± 0.6

withdrawing substituents such as the 4-CF₃ group cause noticeable hypsochromic and electron-donating substituents like (-N(CH₃)₂, -N(Ph)₂) cause noticeable bathochromic shifts of the π - π^* band, respectively.

The photo-luminescent properties of compounds C₁-C₂₇ (in acetonitrile solution) have been investigated and figures 2-4 present the emission spectroscopic data. Likewise, table 1 presents the emission bands. Compounds carrying groups with varying electro-negativity exhibit varying photo-luminescent properties in solution at room temperature. When the substituent groups are modified, the average emission levels of these compounds can be estimated from 273 to 865 nm. Only a single band is noticed in the fluorescence (emission) spectrum of complex C₁₃, while two bands are detected in compounds C₁, C₂, C₃, C₅, C₉, C₁₁, C₁₉, C₂₃, C₂₅ and C₂₇, three bands are detected in compounds C₄, C₆, C₈, C₁₄, C₁₅, C₁₆, C₁₇, C₂₀ and C₂₆ and four bands are detected in compounds C₇, C₁₈, C₂₁ and C₂₂. In C₁₃, only a broad band at 853 nm is seen when excited at 295 nm. For compounds C₁, C₂, C₃, C₅, C₉, C₁₁, C₁₉, C₂₃, C₂₅ and C₂₇, their photo-luminescent spectra display two bands, a low-intensity band at 405 nm and another with higher intensity at 704 nm for C₁, 379 and 776 nm for C₂, 394 and 792 nm for C₃, 547 and 683 nm for C₅, 341 and 747 nm for C₉, 454 and 856 nm for C₁₀, 409 and 856 nm for C₁₉, 391 and 699 nm for C₂₃, 474 and 850 nm for C₂₅ and 565 and 848 nm for C₂₇, respectively, when being excited at around 320 nm. Compounds C₄, C₆, C₈, C₁₁, C₁₂, C₁₄, C₁₅, C₁₆, C₁₇, C₂₀, C₂₄ and C₂₆ show multiple emission behaviours in their spectra, with emission maxima at around 273, 630 and 859 nm upon excitation at 300 nm, whereas the complexes C₇, C₁₈, C₂₁ and C₂₂ show maximal fluorescence with four emission bands at 294, 359, 451 and 717 nm for C₇, 361, 580, 737 and 865 nm for C₁₈, 358, 578, 732 and 869 nm for C₂₁ and 365, 680, 743 and 855 nm for C₂₂ upon excitation at 305 nm. On account of the different substituents at the terpyridine unit, their emission peaks show variations. All of them not only exhibit photo-luminescent properties with high emission but also change the maximum emission peaks from 305 to 856 nm due to the substituent groups.

A strong absorption band for C₁-C₂₇ is due to the π - π^* transitions of a conjugate backbone with maximum absorption λ in the range of 300-869 nm. Moreover, due to the presence of a similar central terpyridine nucleus for all the compounds, the spectral shapes/curves are identical in the UV-Vis (absorption) spectra. It is noteworthy, that the difference in wavelengths and strength of absorption is attributable solely to the influence of the 4-alkylphenyl moieties at the 4'-position of 2,2':6'',2-terpyridine nucleus. The photo-luminescent properties of the complexes (C₁-C₂₇) were then analysed at their corresponding wavelengths of excitation. Compounds having maximum bands showed a maximum emission at higher wavelengths relative to other compounds in the series. This common trend can be attributed to the various configurations of the alkyl groups in solution. These complexes (C₁-C₂₇) also display blue fluorescence due to the presence of their maximum emission wavelengths in the blue region of the visible spectrum, close to most previously recorded terpyridine complexes [65]. The terpyridine ring's structure and substitution pattern are thought to be responsible for certain compounds' blue fluorescence. Aryl groups that exist at *p*-position terpyridine form the conjugated backbone and are primarily responsible for photon absorption. As a result, the substitution of alkyl-aryl groups at 4-position can be assumed to have some effect on physico-chemical properties. It is apparent from the results that changing the length of the alkyl group substantially affects emission strength without a large red- or blue-shift in the emission wavelength, and the replacement of the electron-donating groups (EDG) for the conjugated backbone of these compounds can be used to modify the emission intensity. It is therefore anticipated that by adjusting the 4-aryl terpyridine ring substituent, the emission intensity can be changed, which is very useful for controlling the luminescence and optoelectronic properties of the organic light-emitting diodes (OLEDs) based on related fluorescent compounds.

The SAR studies revealed that the different substituents on ligands are responsible for controlling bioactivities (figure 5). The finding regarding biological aspects of metal complexes shows that the electron-withdrawal substituent on the ligand will boost the anti-bacterial function of the original compound, while the case is reversed for electron-releasing substituents. Such a pattern indicates that the substituents can efficiently regulate the complex's anti-bacterial function. Bulky benzene ring substituents, such as a lipophilic methyl group, have not enhanced the biological activity of parent's analogues. This supports the favourable electron-withdrawal substituent at position 4 to allow the complex structure to become more active. The strong anti-microbial activity observed may be due to the metal centre's nuclearity in the complex; dinuclear centres are usually more active than mononuclear ones. Similar to metal salts and the corresponding ligands, both complexes have anti-bacterial activity against *P. aeruginosa* and *E. coli*, which can be linked to the concept of chelation, where the chelation of metal ions and ligands decreases the polarity of the metal ion mainly due to the partial sharing of its positive charge with the donor groups and potential *p*-electron delocalization

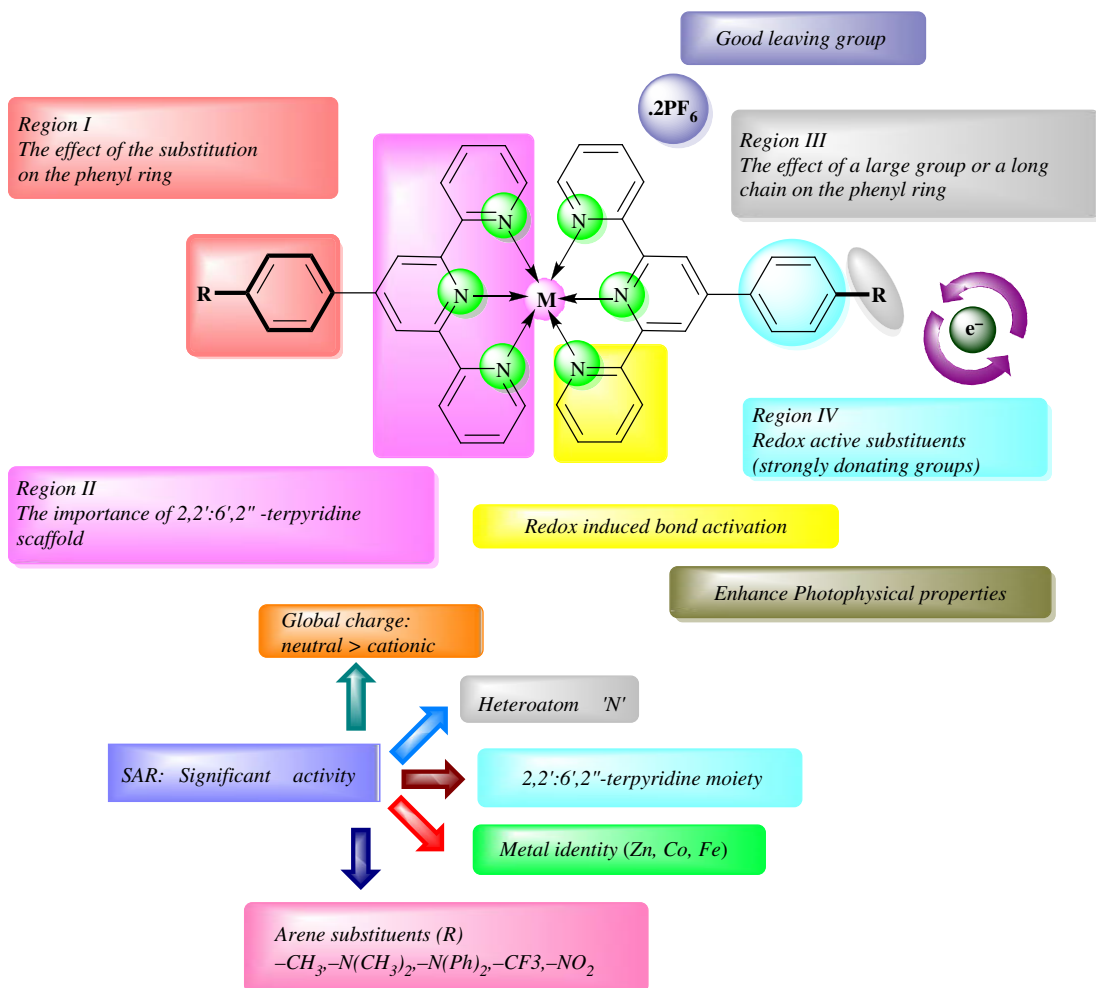


Figure 5. Structure–activity relationship of the synthesized terpyridine-based ligands and metal complexes.

within the entire chelate. In addition, the chelate cycle increases the liposolubility of central metal according to the concept of similarity and inter-miscibility, thereby promoting its permeation through the lipid layer of cell membranes and thus preventing enzyme activity resulting in excellent anti-bacterial properties.

3.44. Docking analysis

In the current study, molecular modelling studies were carried out using a molecular operating environment (MOE) program package for synthetic terpyridine derivatives (**L**₁–**L**₉) against shikimate dehydrogenase and penicillin-binding protein by targeting their active sites and examining the binding poses assumed by the ligands. Computational analysis of designed inhibitors was performed via docking simulations to evaluate the binding orientation, affinity and the binding energy of the tested inhibitors. Potential isolated binding sites of target shikimate dehydrogenase and penicillin-binding proteins were analysed by MOE software. The possible binding sites of ligand molecules at shikimate dehydrogenase are: Met1, Glu2, Thr3, Tyr4, Ile29, Glu30, His31, Pro32, Gly54, Gly55, Gly57, Glu74, Leu75, Thr76, Glu77, Arg78, Ala79, Ala80, Leu81, Ala82, Net89, Leu91, Leu97, Asp99, Asn100, Thr101, Asp102, Gly103, Val104, Leu107, Arg132, Gly133, Val134, Leu135, Leu136, Pro137, Leu139, Ser140, Leu141, Asp142, Phe162, His164, Thr165, His247, Leu250, Leu251, Gly254 (figure 6a); and at penicillin-binding proteins are: Arg408, Leu413, Asn417, Arg418, Phe421, Gly422, Pro424, Thr425, Leu437, Pro438, Asp440, Arg463, Lys470, Net474, Lys496, Glu497, Pro497, Asn501, Thr665, Gly666, Glu694, Glu695, Val696, Pro697, Ala698, Asp698, Tyr700, Gly701, Trp702, Ala734, Asn735, Val896 (figure 6b).

The possible strength of ligand–protein interaction was calculated based on minimal binding energy and scoring efficiency. ‘Grid point’ was allocated to the energy of interaction between the compound and

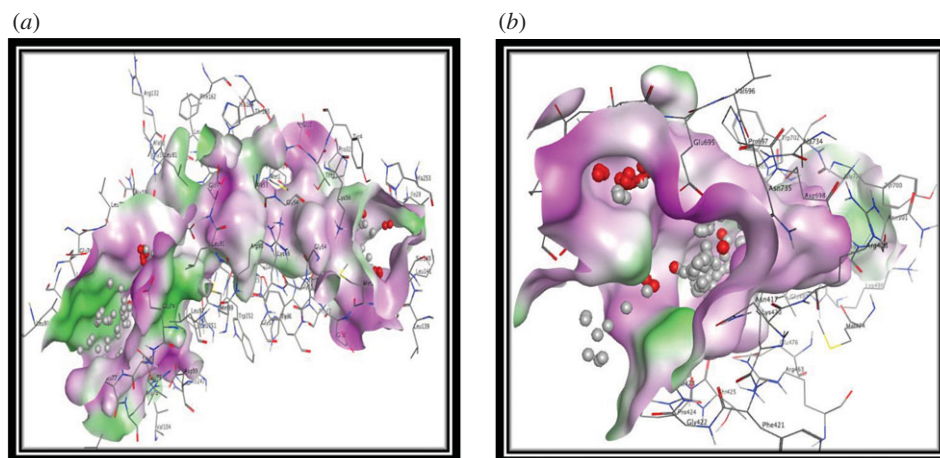


Figure 6. Three-dimensional docking pose of (a) shikimate dehydrogenase and (b) penicillin-binding protein having active binding sites.

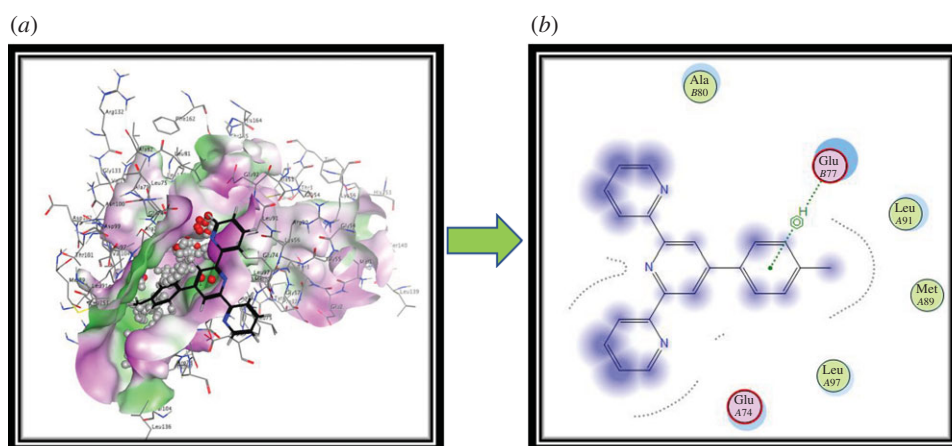


Figure 7. Molecular modelling views and information of ligand L_1 association with atoms of shikimate dehydrogenase as the target (PDB ID: 3DON) performed by MOE software. (a) Three-dimensional interaction and (b) two-dimensional interaction with amino acid residues.

the target enzyme. Finally, those synthesized ligands were docked with the target molecules active sites. In short, at every simulation stage, the interaction energy of ligands and proteins was determined using atomic affinity potentials, calculated on a grid, while the remaining parameters were set as usual. The effects of molecular docking were clustered, and the lowest binding energy cluster was assessed as a binding representative state. The target proteins were considered successfully docked with ligand molecules as minimum binding energies were released. Each of the compounds has been checked to collect information on binding interactions that can be highly important for target inhibition. Binding interaction diagrams were obtained using the MOE ligand interaction analysis tool.

Among the L series, it was observed that against shikimate dehydrogenase (PDB ID: 3DON), the most active compound is ligand L_1 ($-5.97 \text{ kcal mol}^{-1}$) manifesting significant binding affinity. It develops the hydrophobic π - π stacked type associations with Glu77 and Glu74 of catalytic triad amino acid residues. Ala80, Leu91, Met89 and Leu87 amino acid residues of active pockets of shikimate dehydrogenase develop the hydrophobic π - π stacked, π -sulfur, hydrogen bond and hydrophobic π -alkyl type interactions, as shown in figure 7a,b.

Similarly, for penicillin-binding protein (PDB ID: 1VQQ), ligand L_1 ($-5.743 \text{ kcal mol}^{-1}$) showed the best activity (table 3). Additionally, the derivative L_1 reveals its inhibitory potential against penicillin-binding protein by forming fruitful types of electrostatic interactions. This compound builds up hydrophobic π -alkyl type interactions with Glu695 of the acyl-binding pocket inside the penicillin-binding protein. Asn735 of the peripheral anionic site (PAS) develops hydrophobic π - π stacked type associations inside the pocket of penicillin-binding protein. This ligand also exhibits π -lone pair,

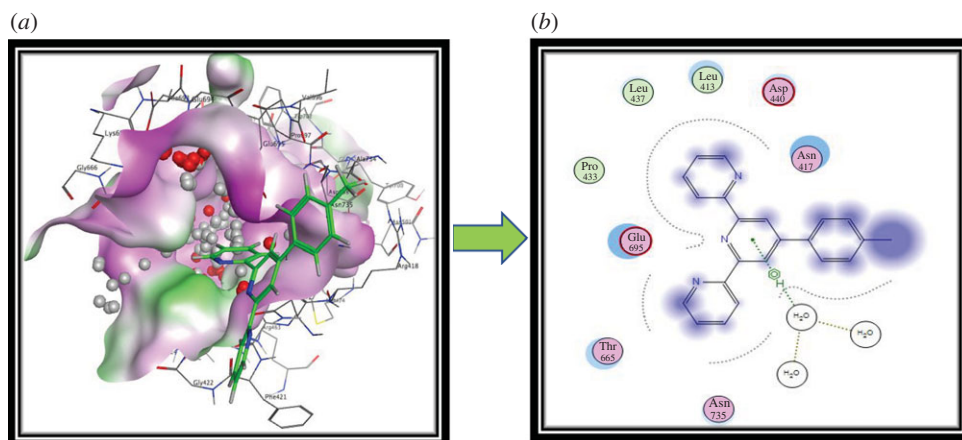


Figure 8. Molecular modelling views (best pose has been shown) and information of ligand L_1 interaction with atoms of penicillin-binding protein as the target (PDB ID: 1VQQ) performed by MOE software. (a) Three-dimensional interaction and (b) two-dimensional interaction with amino acid residues.

Table 3. Energy values obtained by docking analysis of some of the synthesized ligands (L_1 – L_9) against shikimate dehydrogenase and penicillin-binding protein target molecule.

compound no.	shikimate dehydrogenase lowest binding energy ΔG (kcal mol $^{-1}$)	penicillin-binding protein lowest binding energy ΔG (kcal mol $^{-1}$)
L_1	–5.970	–5.743
L_2	–5.421	–5.283
L_3	–5.413	–5.237
L_4	–3.749	–4.437
L_5	–5.050	–4.859
L_6	–4.849	–4.664
L_7	–4.557	–4.590
L_8	–4.834	–4.010
L_9	–4.783	–4.964
standard	–5.010 (NSC)	–8.180 (gentamycin)

hydrophobic π – π T-shaped and hydrophobic π -alkyl type associations with the Asn417, Asp440, Leu413, Leu437, Pro438 and Thr665 amino acid residues inside the active pockets of penicillin-binding protein as shown in figure 8a,b.

Overall, it has been observed that these ligands (L_2 – L_9) showed moderate to good binding affinity with the target proteins. However, it is observed that L_1 showed maximum binding affinities with shikimate dehydrogenase as compared with penicillin-binding proteins (figures 7 and 8). Geometric protein arrangement of amino acid residues inappropriate and disallowed regions shows the value of the target proteins.

3.45. Density functional theory (computational study)

3.45.1. Frontier molecular orbitals analysis

The energies and extents of the highest occupied molecular orbital (HOMO) and lowest unoccupied molecular orbital (LUMO) in a molecule are related to its ability to donate and accept an electron and the energy gap between these orbitals tells the stability, chemical reactivity and photoabsorption behaviour of the compounds [83]. Different functional groups in compounds can change the positions and energy gap of HOMO-LUMO, which noticeably affects the charge transfer transitions. This change in the energy band gap can be exploited in tuning photophysical and chemical reactivity features of the

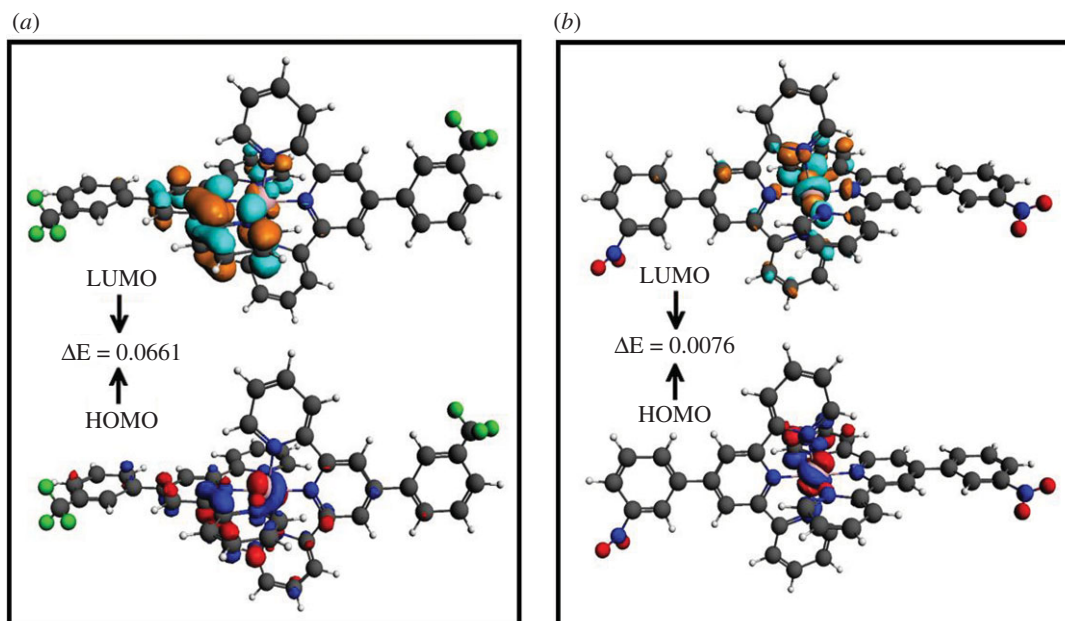


Figure 9. DFT-B3LYP* (DZ) calculated frontier molecular orbitals (FMOs) of (a) C_{15} and (b) C_{24} .

Table 4. DFT-B3LYP* (DZ) calculated values of E_{LUMO} , E_{HOMO} and $E_{HOMO}-E_{LUMO}$ gap (ΔE) of representative complexes experimental λ_{max}

compound code	E_{LUMO} (Hartee)	E_{HOMO} (Hartee)	$E_{LUMO}-E_{HOMO}$ gap ΔE (Hartee)	λ_{max} (nm) (experimental)
C_{13}	-0.1505	-0.2121	0.0616	570
C_{14}	-0.1088	-0.1235	0.0147	526
C_{15}	-0.2257	-0.2918	0.0661	568
C_{22}	-0.1709	-0.2136	0.0427	580
C_{23}	-0.1244	-0.1253	0.0009	535
C_{24}	-0.0881	-0.0957	0.0076	575

compounds. DFT-B3LYP* (DZ) calculated values of E_{LUMO} , E_{HOMO} and $E_{HOMO}-E_{LUMO}$ gap (ΔE) of the metal complexes (C_{13} , C_{14} , C_{15} , C_{22} , C_{23} , and C_{24}) are given in table 4. Frontier molecular orbitals participating in electron transfer in the complexes are depicted in figure 9 and electronic supplementary material, whereas experimentally determined λ_{max} for all the compounds are shown in table 4. ΔE of the C_{15} was found to be higher among all corresponding compounds whereas C_{23} showed the smallest energy gap. Hence, tuning the energy band gap by varying the functional group can cause variation in absorptive properties (explained further in UV-Vis analysis section).

3.46. UV-Vis analysis

UV-Vis spectra of representative complexes of both terpyridine ligands were calculated by DFT-B3LYP* (DZ) methods to analyse the electronic absorption patterns in the complexes. A comparison of experimental UV-Vis and calculated spectra of compounds C_{15} and C_{24} is given in figure 10, which indicates good agreement between the two for both complexes.

The experimental absorption spectrum showed the typical metal to ligand charge transfer (MLCT) transition of the Fe(II)-terpyridine system (C_{15}) at λ_{max} 568 nm, while in the calculated spectrum, it was observed at 572 nm. An intense absorption band in the calculated spectrum of Fe(II) complex (C_{24}) was observed at 578 nm (experimental λ_{max} = 575 nm) which is due to an MLCT transitions in the complex. A redshift in theoretical and experimental absorption spectrum is attributed to the low energy gap for C_{24} (ΔE = 0.0076 Hartee) as compared with C_{15} (ΔE = 0.0661 Hartee). Hence, bandgap tuning by different substituents can alter the absorption behaviours and photophysical characteristics.

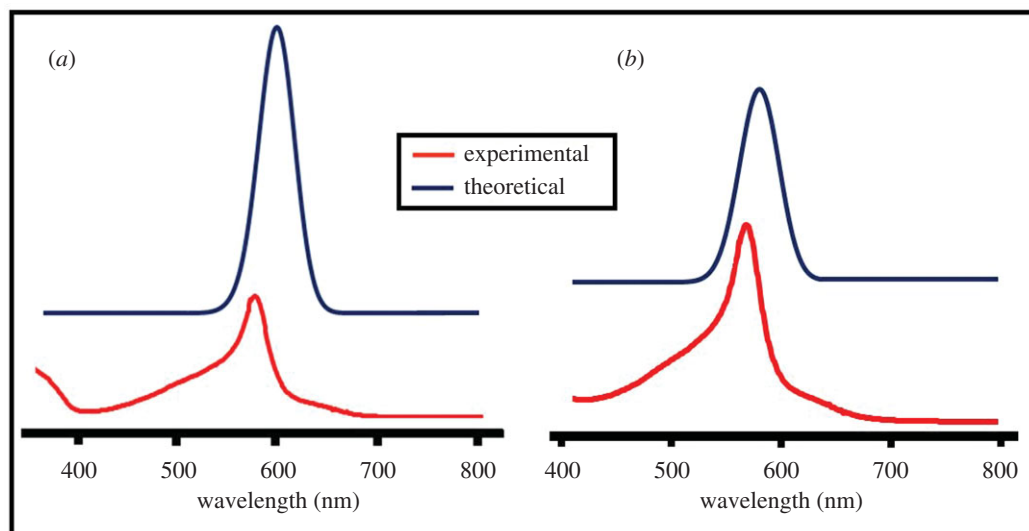


Figure 10. Experimental and DFT-B3LYP* (DZ) calculated UV-Vis spectra of representative metal complexes of ligands L_5 and L_8 : (a) C_{15} and (b) C_{24} .

Table 5. The DFT-B3LYP* (DZ) calculated chemical reactivity parameters of representative complexes.

compound code	electron affinity (EA)	ionization potential (IP)	electro-negativity (χ)	electro-philicity (ω)	chemical potential (μ)	global hardness (η)	global softness (σ)
C_{13}	0.1505	0.2121	0.1813	0.533599	-0.1813	0.0308	16.23377
C_{14}	0.1088	0.1235	0.11615	0.917743	-0.11615	0.00735	68.02721
C_{15}	0.2257	0.2918	0.25875	1.012883	-0.25875	0.03305	15.12859
C_{22}	0.1709	0.2136	0.19225	0.865575	-0.19225	0.02135	23.4192
C_{23}	0.1244	0.1253	0.12485	1.731947	-0.12485	0.0045	111.111
C_{24}	0.0881	0.0957	0.0919	1.111264	-0.0919	0.0038	131.5789

3.47. Chemical reactivity parameters

The chemical reactivity parameters indicate the capability of structures to be stabilized by attracting charge from the environment [84]. The chemical reactivity characteristics of the compounds can be evaluated by parameters such as ionization potential, electron affinity, electro-negativity, electro-philicity, chemical potential, global hardness and global softness [83]. These parameters were calculated for the metal complexes (C_{13} , C_{14} , C_{15} , C_{22} , C_{23} and C_{24}) and are reported in table 5. The chemical reactivity characteristics electro-negativity ($\chi = IP + EA/2$), chemical hardness ($\eta = IP - EA/2$) and chemical potential ($\mu = E_{LUMO} + E_{HOMO}/2$) are calculated according to Koopmans Theorem [85]. IP ($-E_{HOMO}$) is the ionization potential and EA ($-E_{LUMO}$) is the electron affinity. Global softness (σ) can be evaluated by the equation ($\sigma = 1/2\eta$) [86]. The electro-philicity index (ω) for measuring electrophilic strength was calculated by ($\omega = \mu^2/2\eta$) in accordance to Parr *et al.* [87,88].

A small energy gap indicates the compound to be soft and reactive, while a large energy gap indicates the molecule to be hard and not react easily [89]. The complexes C_{14} , C_{23} and C_{24} have shown greater softness character (68, 111 and 131, respectively) thereby tending to be more reactive, which is attributed to the lower bandgap values obtained. In addition, these compounds have low values of ionization potential indicating higher reactivities. Higher values of global hardness than softness indicate less reactivity and higher stability and from the calculated values of global hardness, the most thermally and kinetically stable compound is C_{22} . The calculated negative value of chemical potential shows that it is comparatively easy for the compounds to gain electrons from the environment. However, compounds are found to have greater charge transferability and most of the compounds are found to be reactive.

Strong charge transfers by FMO analysis, also indicated in the UV-Vis spectra of representative complexes, indicated that representative compounds could show potential activities against microbial strains. Tuning the bandgap by substituting different functional groups can alter reactivity characteristics along with photophysical properties as described in the UV-Vis analysis. It is evident from the chemical reactivity studies that these compounds can be used as efficient anti-microbial and biological agents for further studies.

4. Conclusion

We have presented the spectroscopic, photophysical, and anti-microbial studies of Zn(II), Co(II) and Fe(II) complexes of the variously substituted 2,2':6',2''-terpyridine motif. New substrates of symmetrically substituted *p*-aryl-2,2':6',2''-terpyridine have been efficiently prepared by employing a multi-step Kröhnke methodology. The resulting terpyridine-based complexes exhibit interesting photoluminescent properties with strong emission upon excitation at the corresponding absorption maximum. Investigations carried on $[M(\text{tpy-X})]^{2+}$ complexes (where X is the substituent in the 4' position of 2,2':6',2''-terpyridine) have revealed that introduction of either electron-donating ($-\text{CH}_3$, $-\text{N}(\text{CH}_3)_2$, $-\text{N}(\text{Ph})_2$, $-\text{OCH}_3$) or electron-withdrawing ($-\text{NO}_2$, $-\text{CF}_3$) groups onto the aryl-terpyridine scaffold alters absorbance as well as fluorescence properties and thus resulted in bathochromic shifted and structurally varied absorption and emission spectra. In addition, we have observed that the introduction of d-block transition metals (Zn, Co, Fe) into the terpyridine derivatives modified their absorption and emission properties as compared with terpyridine ligands (L_1 – L_9), and most complexes (C_1 – C_{27}) showed red-shifted absorption and emission spectra of varied appearance in contrast with the 2,2':6',2''-terpyridines. Many of the new compounds have interesting photo-luminescent properties with high emissions. Importantly, almost all the functionalized terpyridine complexes display longer emission λ and they are stronger emissive in contrast with the unsubstituted 2,2':6',2''-terpyridine.

The ligands and complexes were also evaluated for their anti-microbial potential (*in vitro*). The analysis revealed that the complexes (C_1 – C_{27}) exhibited more potent activity than free ligands (L_1 – L_9). Overall, the entire compounds exhibited moderate to excellent anti-microbial activities. These results provide new possibilities for therapeutic purposes. The experimental results complemented with *in silico* studies provided insights into structure–property relationships. We are quite confident that the reported structures may find applications in organic electronics as well as medicines as potential materials and this will be the target of our future investigations. The investigation permitted the selection of materials with the most promising properties with special emphasis on the nature of the substituents.

Data accessibility. All the UV, fluorescence, mass spectra, biological evaluation images and DFT images of selected compounds can be found in the electronic supplementary material.

Authors' contributions. E.U.M. was involved in main idea, supervision and final writing the manuscript. M.M. was involved in co-supervision. A.S. was involved in co-supervision. S.F. was involved in experimental work performance and first-draft preparation. A.N. was involved experimental work performance and first-draft preparation. N.N. was involved in data analysis and collection, software. N.F. performed enzyme inhibition experiments. S.K. performed DFT studies. A.A.A. performed DFT studies. M.N.Z. performed molecular docking studies. B.A.K. was involved in mass spectrometry analysis. All authors gave final approval for publication.

Competing interests. There are no conflicts of interest to declare.

Funding. The Higher Education Commission of Pakistan (HEC) under project no. NRPU-6484 funded this study. M.M. gratefully acknowledges the financial support provided by the Ferdowsi University of Mashhad.

Acknowledgements. The authors are highly grateful to Dr. Renhao Dong, Department of Advanced Materials, Dresden University, Germany for his kind help in spectroscopic measurements.

References

- Schubert U, Winter A, Newkome GR. 2012 *Terpyridine-based materials: for catalytic, photoelectronic and life science applications*. Weinheim, Germany: Wiley-VCH.
- Husson J, Guyard L. 2018 4'-(5-Methylfuran-2-yl)-2,2':6',2''-terpyridine: a new ligand obtained from a biomass-derived aldehyde with potential application in metal-catalyzed reactions. *Molbank* **2018**, M1032. (doi:10.3390/M1032)
- Momeni BZ, Heydari S. 2015 Design of novel copper (II) and zinc (II) coordination polymers based on the 4'-functionalized terpyridines. *Polyhedron*. **97**, 94–102. (doi:10.1016/j.poly.2015.05.019)
- Trokowski R, Akine S, Nabeshima T. 2008 Synthesis, characterization and molecular recognition of a bis-platinum terpyridine dimer. *Chem. Commun.* **7**, 889–890. (doi:10.1039/b716459a)
- Yam VWW, Hui CK, Yu SY, Zhu N. 2004 Syntheses, luminescence behavior, and assembly reaction of tetraalkynylplatinate(II) complexes: crystal structures of $[\text{Pt}(\text{tBu}_3\text{trpy})(\text{C}:\text{CC}_5\text{H}_4\text{N})\text{Pt}(\text{tBu}_3\text{trpy})](\text{PF}_6)_3$ and

- [Pt₂Ag₄(C:CC:CC₆H₄CH₂⁻⁴)₈(THF)₄]. *Inorg. Chem.* **43**, 812–821. (doi:10.1021/ic0348771)
6. Di Nicola C, Marchetti F, Pettinari C, Skelton BW, White AH. 2007 Synthesis and structural characterization of adducts of silver(I) nitrate with ER₃ (E= P, As, Sb; R= Ph, cy, o-tolyl, mes) and oligodentate aromatic bases derivative of 2, 2'-bipyridyl, L, AgNO₃:ER₃:L(1:1:1). *Inorg. Chim. Acta* **360**, 1433–1450. (doi:10.1016/j.ica.2006.07.017)
 7. Müller J, Freisinger E, Lax P, Megger DA, Polonius FA. 2007 Interaction of Pt(II) and Pd(II) complexes of terpyridine with 1-methylazoles: a combined experimental and density functional study. *Inorg. Chim. Acta* **360**, 255–263. (doi:10.1016/j.ica.2006.07.031)
 8. Zhang SS, Zhan SZ, Li M, Peng R, Li D. 2007 A rare chiral self-catenated network formed by two cationic and one anionic frameworks. *Inorg. Chem.* **46**, 4365–4367. (doi:10.1021/ic070250h)
 9. Field JS, Haines RJ, Ledwaba LP, McGuire Jr R, Munro OQ, Low MR, McMillin DR. 2007 Synthesis, electrochemistry and luminescence of [Pt(4'-(R)trpy)(CN)]⁺ (R= Ph, o-CH₃C₆H₄, o-ClC₆H₄, or o-CF₃C₆H₄; trpy= 2,2':6',2''-terpyridine): Crystal structure of [Pt(4'-(Ph)trpy)(CN)]BF₄·CH₃CN. *Dalton Trans.* **2**, 192–199. (doi:10.1039/B611244G)
 10. Shikhova E, Danilov EO, Kinayyigit S, Pomestchenko IE, Tregubov AD, Camerel F, Retailleau P, Ziessel R, Castellano FN. 2007 Excited-state absorption properties of platinum(II) terpyridyl acetylides. *Inorg. Chem.* **46**, 3038–3048. (doi:10.1021/ic0618652)
 11. Fan Y, Zhu YM, Dai FR, Zhang LY, Chen ZN. 2007 Photophysical and anion sensing properties of platinum(II) terpyridyl complexes with phenolic ethynyl ligands. *Dalton Trans.* **35**, 3885–3892. (doi:10.1039/b707797a)
 12. Alcock NW, Barker PR, Haider JM, Hannon MJ, Painting CL, Pikramenou Z, Plummer EA, Rissanen K, Saarenketo P. 2000 Red and blue luminescent metallo-supramolecular coordination polymers assembled through π-π interactions. *J. Chem. Soc., Dalton Trans.* **9**, 1447–1462. (doi:10.1039/b000871k)
 13. Liu C, Jiang J, Li J, Liang X, Zhou Y, Chen H, Ma Z. 2020 Synthesis, structural characterization and antiproliferative potential of copper 4'-phenyl-terpyridine complexes constructed from building block reaction. *Polyhedron*. **182**, 114465. (doi:10.1016/j.poly.2020.114465)
 14. Ma Z, Xing Y, Yang M, Hu M, Liu B, da Silva MFCG, Pombeiro AJ. 2009 The double-helicate terpyridine silver (I) compound [Ag₂L₂](SO₃CF₃)₂ (L= 4'-phenyl-terpyridine) as a building block for di- and mononuclear complexes. *Inorg. Chim. Acta* **362**, 2921–2926.
 15. Ma Z, Cao Y, Li Q, da Silva MFCG, da Silva JF, Pombeiro AJ. 2010 Synthesis, characterization, solid-state photo-luminescence and anti-tumor activity of zinc(II) 4'-phenyl-terpyridine compounds. *J. Inorg. Biochem.* **104**, 704–711. (doi:10.1016/j.jinorgbio.2010.03.002)
 16. Ma Z, Lu W, Liang B, Pombeiro AJ. 2013 Synthesis, characterization, photoluminescent and thermal properties of zinc(II) 4'-phenyl-terpyridine compounds. *New J. Chem.* **37**, 1529–1537. (doi:10.1039/c3nj41176a)
 17. Ma Z, Wang Q, Alegria ECBA, da Silva MFCG, Martins LMDRS, Telo JP, Correia I, Pombeiro AJ. 2019 Synthesis and structure of copper complexes of a N₄O₂ macrocyclic ligand and catalytic application in alcohol oxidation. *Catalysts* **9**, 424. (doi:10.3390/catal9050424)
 18. Constable EC, Lewis J, Liptrot MC, Raitby PR. 1990 The coordination chemistry of 4'-phenyl-2, 2':6',2''-terpyridine; the synthesis, crystal and molecular structures of 4'-phenyl-2,2':6',2''-terpyridine and bis(4'-phenyl-2,2':6',2''-terpyridine) nickel(II) chloride decahydrate. *Inorg. Chim. Acta* **178**, 47–54. (doi:10.1016/S0020-1693(00)88132-3)
 19. Ma Z, Ran G. 2011 Syntheses and structural characterization of cadmium complexes constructed from a tetrakis (3-pyridylmethyl) functionalized ligand. *J. Coord. Chem.* **64**, 1446–1455. (doi:10.1080/00958972.2011.572967)
 20. Ma Z, Wei L, Alegria EC, Martins LM, da Silva MFCG, Pombeiro AJ. 2014 Synthesis and characterization of copper(II) 4'-phenyl-terpyridine compounds and catalytic application for aerobic oxidation of benzylic alcohols. *Dalton Trans.* **43**, 4048–4058. (doi:10.1039/C3DT53054J)
 21. Halcrow MA. 2005 The synthesis and coordination chemistry of 2,6-bis(pyrazolyl) pyridines and related ligands—versatile terpyridine analogues. *Coord. Chem. Rev.* **249**, 2880–2908. (doi:10.1016/j.ccr.2005.03.010)
 22. Padhy H, Sahu D, Chiang IH, Patra D, Kekuda D, Chu CW, Lin HC. 2011 Synthesis and applications of main-chain Ru(II) metallo-polymers containing bis-terpyridyl ligands with various benzodiazole cores for solar cells. *J. Mater. Chem.* **21**, 1196–1205. (doi:10.1039/C0JM02532A)
 23. Liu M, Ye Z, Wang G, Yuan J. 2012 Synthesis and time-gated fluorometric application of a europium(III) complex with a borono-substituted terpyridine polyacid ligand. *Talanta* **91**, 116–121. (doi:10.1016/j.talanta.2012.01.028)
 24. Dobra R, Würthner F. 2002 Photoluminescent supramolecular polymers: metal-ion directed polymerization of terpyridine-functionalized perylene bisimide dyes. *Chem. Commun.* **17**, 1878–1879. (doi:10.1039/B205478G)
 25. Yutaka T, Mori I, Kurihara M, Mizutani J, Tamai N, Kawai T, Irie M, Nishihara H. 2002 Photoluminescence switching of azobenzene-conjugated Pt(II) terpyridine complexes by trans–cis photoisomerization. *Inorg. Chem.* **41**, 7143–7150. (doi:10.1021/ic0260116)
 26. Ion AE, Cristian L, Voicescu M, Bangesh M, Madalan AM, Bala D, Mihailciuc C, Nica S. 2016 Synthesis and properties of fluorescent 4'-azulenyl-functionalized 2,2':6',2''-terpyridines. *Beilstein J. Org. Chem.* **12**, 1812–1825. (doi:10.3762/bjoc.12.171)
 27. Saccone D, Magstris C, Barbero N, Quagliotto P, Barolo C, Viscardi G. 2016 Terpyridine and quarter pyridine complexes as sensitizers for photovoltaic applications. *Materials* **9**, 137. (doi:10.3390/ma9030137)
 28. Sakamoto R, Wu KH, Matsuoka R, Maeda H, Nishihara H. 2015 π-Conjugated bis (terpyridine) metal complex molecular wires. *Chem. Soc. Rev.* **44**, 7698–7714. (doi:10.1039/C5CS00081E)
 29. Schwarz G, Hasslauer I, Kurth DG. 2014 From terpyridine-based assemblies to metallo-supramolecular polyelectrolytes (MEPEs). *Adv. Colloid Interfac.* **207**, 107–120. (doi:10.1016/j.cis.2013.12.010)
 30. Sakamoto R, Katagiri S, Maeda H, Nishihara H. 2013 Bis(terpyridine) metal complex wires: excellent long-range electron transfer ability and controllable intrawire redox conduction on silicon electrode. *Coord. Chem. Rev.* **257**, 1493–1506. (doi:10.1016/j.ccr.2012.08.025)
 31. Schubert U, Hofmeier H, Newkome GR. 2006 *Modern terpyridine chemistry*. Weinheim, Germany: Wiley-VCH.
 32. Constable EC. 2007 2,2':6',2''-Terpyridines: from chemical obscurity to common supramolecular motifs. *Chem. Soc. Rev.* **36**, 246–253. (doi:10.1039/B601166G)
 33. Schubert US, Eschbaumer C. 2002 Macromolecules containing bipyridine and terpyridine metal complexes: towards metallo-supramolecular polymers. *Angew. Chem. Int. Ed.* **41**, 2892–2926. (doi:10.1002/1521-3773(20020816)41:16<2892::AID-ANIE2892>3.0.CO;2-6)
 34. Hofmeier H, Schubert US. 2004 Recent developments in the supramolecular chemistry of terpyridine–metal complexes. *Chem. Soc. Rev.* **33**, 373–399. (doi:10.1039/B400653B)
 35. Medlycott EA, Hanan GS. 2005 Designing tridentate ligands for ruthenium(II) complexes with prolonged room temperature luminescence lifetimes. *Chem. Soc. Rev.* **34**, 133–142. (doi:10.1039/b316486c)
 36. Yu SC, Kwok CC, Chan WK, Che CM. 2003 Self-assembled electroluminescent polymers derived from terpyridine-based moieties. *Adv. Mater.* **15**, 1643–1647. (doi:10.1002/adma.200305002)
 37. Zhang X, Jin YH, Diao HX, Du FS, Li ZC, Li FM. 2003 Synthesis of bismaleimides bearing electron-donating chromophores and their fluorescence behavior during copolymerization. *Macromolecules.* **36**, 3115–3127. (doi:10.1021/ma0205111)
 38. Pohl R, Montes VA, Shinar J, Anzenbacher P. 2004 Red–green–blue emission from Tris (5-aryl-8-quinolinolate) Al(III) complexes. *J. Org. Chem.* **69**, 1723–1725. (doi:10.1021/jo035602q)
 39. Botha E, Landman M, Van Rooyen PH, Erasmus E. 2018 Electronic properties of ferrocenyl-terpyridine coordination complexes: an electrochemical and X-ray photoelectron spectroscopic approach. *Inorg. Chim. Acta* **482**, 514–521. (doi:10.1016/j.ica.2018.04.013)
 40. Mishra A, Mena-Osteritz E, Bäuerle P. 2013 Synthesis, photophysical and electrochemical characterization of terpyridine-functionalized dendritic oligothiophenes and their Ru(II) complexes. *Beilstein J. Org. Chem.* **9**, 866–876. (doi:10.3762/bjoc.9.100)
 41. Colinas IR, Rojas-Andrade MD, Chakraborty I, Oliver SR. 2018 Two structurally diverse Zn-based coordination polymers with excellent antibacterial activity. *CrystEngComm.* **20**, 3353–3362. (doi:10.1039/C8CE00394G)
 42. Urquiza NM *et al.* 2013 Inhibition behavior on alkaline phosphatase activity, antibacterial and antioxidant activities of ternary methimazole–

- phenanthroline–copper(II) complex. *Inorg. Chim. Acta* **405**, 243–251. (doi:10.1016/j.ica.2013.05.022)
43. Montazerzohori M, Yadegari S, Naghiha A. 2014 Synthesis, characterization, electrochemical behavior and antibacterial/antifungal activities of [Cd(II)₂] complexes with a Schiff base ligand. *J. Serb. Chem. Soc.* **79**, 793–804. (doi:10.2298/JSC130520110M)
 44. Wang X, Li R, Liu A, Yue C, Wang S, Cheng J, Li J, Liu Z. 2019 Syntheses, crystal structures, antibacterial activities of Cu(II) and Ni(II) complexes based on terpyridine polycarboxylic acid ligand. *J. Mol. Struct.* **1184**, 503–511. (doi:10.1016/j.molstruc.2019.02.072)
 45. Salehi M, Rahimifar F, Kubicki M, Asadi A. 2016 Structural, spectroscopic, electrochemical and antibacterial studies of some new nickel(II) Schiff base complexes. *Inorg. Chim. Acta.* **443**, 28–35. (doi:10.1016/j.ica.2015.12.016)
 46. Chohan ZH, Naseer MM. 2007 Organometallic based biologically active compounds: Synthesis of mono- and di-ethanolamine derived ferrocenes with antibacterial, antifungal and cytotoxic properties. *Appl. Organomet. Chem.* **21**, 1005–1012. (doi:10.1002/aoc.1313)
 47. Wu XY, Qi HX, Ning JJ, Wang JF, Ren ZG, Lang JP. 2015 One silver(I)/tetrachlorophosphate coordination polymer showing good catalytic performance in the photodegradation of nitroaromatics in aqueous solution. *Appl. Catal. B- Environ.* **168**, 98–104.
 48. Yuan FL, Yuan YQ, Chao MY, Young DJ, Zhang WH, Lang JP. 2017 Deciphering the structural relationships of five Cd-based metal–organic frameworks. *Inorg. Chem.* **56**, 6522–6531. (doi:10.1021/acs.inorgchem.7b00592)
 49. Hollingsworth TS, Hollingsworth RL, Lord RL, Groysman S. 2018 Cooperative bimetallic reactivity of a heterodinuclear molybdenum–copper model of Mo–Cu CODH. *Dalton Trans.* **47**, 10 1017–10 024. (doi:10.1039/C8DT02323A)
 50. Hao Y, Yue C, Jin B, Lv Y, Zhang Q, Li J, Liu Z, Hou H. 2018 Syntheses, structures, luminescent properties and antibacterial activities of seven polymers based on an asymmetric triazole dicarboxylate ligand. *Polyhedron.* **139**, 296–307. (doi:10.1016/j.poly.2017.11.006)
 51. Zhang Q, Yue C, Zhang Y, Lü Y, Hao Y, Miao Y, Li J, Liu Z. 2018 Six metal–organic frameworks assembled from asymmetric triazole carboxylate ligands: synthesis, crystal structures, photoluminescence properties and antibacterial activities. *Inorg. Chim. Acta.* **473**, 112–120. (doi:10.1016/j.ica.2017.12.036)
 52. Paira MK, Mondal TK, Ojha D, Slawin AM, Tiekink ER, Samanta A, Sinha C. 2011 Structures, redox behavior, antibacterial activity and correlation with electronic structure of the complexes of nickel triad with 3-(2-(alkylthio)phenylazo)-2,4-pentanedione. *Inorg. Chim. Acta.* **370**, 175–186. (doi:10.1016/j.ica.2011.01.049)
 53. Patel MN, Dosi PA, Bhatt BS. 2010 Antibacterial, DNA interaction and superoxide dismutase activity of drug based copper(II) coordination compounds. *Polyhedron.* **29**, 3238–3245. (doi:10.1016/j.poly.2010.08.037)
 54. Psomas G, Dendrinou-Samara C, Philippakopoulos P, Tangoulis V, Raptopoulou CP, Samaras E, Kessissoglou DP. 1998 Cull-herbicide complexes: structure and bioactivity. *Inorg. Chim. Acta.* **272**, 24–32. (doi:10.1016/S0020-1693(97)05847-7)
 55. Abdallah SM, Mohamed GG, Zayed M, El-Ela MSA. 2009 Spectroscopic study of molecular structures of novel Schiff base derived from *o*-phthalaldehyde and 2-aminophenol and its coordination compounds together with their biological activity. *Spectrochim Acta A.* **73**, 833–840. (doi:10.1016/j.saa.2009.04.005)
 56. Abdallah SM, Zayed M, Mohamed GG. 2010 Synthesis and spectroscopic characterization of new tetradentate Schiff base and its coordination compounds of NOON donor atoms and their antibacterial and antifungal activity. *Arab. J. Chem.* **3**, 103–113. (doi:10.1016/j.arabj.2010.02.006)
 57. Sabounchei SJ, Bagherjeri FA, Mozafari Z, Boskovic C, Gable RW, Karamian R, Asadbegy M. 2013 Synthesis and characterization of novel simultaneous C and O-coordinated and nitrate-bridged complexes of silver(I) with carbonyl-stabilized sulfonium slides and their antibacterial activities. *Dalton Trans.* **42**, 2520–2529. (doi:10.1039/C2DT31902K)
 58. Palacios-Hernández T, Höpfl H, Sánchez-Salas J, González-Vergara E, Pérez-Benitez A, Quiroz-Alfaro M, Méndez-Rojas M. 2014 *In vitro* antibacterial activity of medofenamate metal complexes with Cd(II), Pb(II), Co(II), and Cu(II). Crystal structures of [Cd(C₁₄H₁₀NO₂Cl₂)₂(CH₃OH)]_n and [Cu(C₁₄H₁₀NO₂Cl₂)₂(C₅H₅N)₂]. *J. Inorg. Biochem.* **139**, 85–92. (doi:10.1016/j.jinorgbio.2014.06.008)
 59. Patel MN, Patidar AP. 2014 DNA interactions and promotion in antibacterial activities of the norfloxacin drug due to formation of mixed-ligand copper(II) complexes. *Monatsh. Chem.* **145**, 369–381. (doi:10.1007/s00706-013-1086-4)
 60. Bobiev G, Sufiev T, Shakhmatov A. 2008 Antibacterial properties of coordination compounds of silver and tryptophan. *Pharm. Chem. J.* **42**, 614–615. (doi:10.1007/s11094-009-0200-8)
 61. Wang F, Wang YT, Yu H, Chen JX, Gao BB, Lang JP. 2016 One unique 1D silver(I)-bromide-thiol coordination polymer used for highly efficient chemiresistive sensing of ammonia and amines in water. *Inorg. Chem.* **55**, 9417–9423. (doi:10.1021/acs.inorgchem.6b01688)
 62. Hu FL, Mi Y, Zhu C, Abrahams BF, Braunstein P, Lang JP. 2018 Stereoselective solid-state synthesis of substituted cyclobutanes assisted by pseudorotaxane-like MOFs. *Angew. Chem.* **130**, 12 878–12 883. (doi:10.1002/ange.201806076)
 63. Ghazal K, Shoaib S, Khan M, Khan S, Rauf MK, Khan N, Badshah A, Tahir MN, Ali I. 2019 Synthesis, characterization, X-ray diffraction study, *in-vitro* cytotoxicity, antibacterial and antifungal activities of nickel(II) and copper(II) complexes with acyl thiourea ligand. *J. Mol. Struct.* **1177**, 124–130. (doi:10.1016/j.molstruc.2018.09.028)
 64. Gao EJ, Feng YH, Su JQ, Meng B, Jia B, Qi ZZ, Peng TT, Zhu MC. 2018 Synthesis, characterization, DNA binding, apoptosis and molecular docking of three Mn(II), Zn(II) and Cu(II) complexes with terpyridine-based carboxylic acid. *Appl. Organomet. Chem.* **32**, 4164. (doi:10.1002/aoc.4164)
 65. Wang J, Hanan GS. 2005 A facile route to sterically hindered and non-hindered 4'-aryl-2,2':6',2''-terpyridines. *Synlett.* **20**, 1251–1254.
 66. Naseri Z, Kharat AN, Banavand A, Bakhoda A, Foroutannejad S. 2012 First row transition metal complexes of thienyl substituted terpyridine: structural, photophysical and biological studies. *Polyhedron.* **33**, 396–403. (doi:10.1016/j.poly.2011.11.060)
 67. Tang WS, Lu XX, Wong KMC, Yam VWW. 2005 Synthesis, photophysics and binding studies of Pt(II) alkynyl terpyridine complexes with crown ether pendant: potential luminescent sensors for metal ions. *J. Mater. Chem.* **15**, 2714–2720. (doi:10.1039/b501644d)
 68. Anthonysamy A, Balasubramanian S, Shanmugaiah V, Mathivanan N. 2008 Synthesis, characterization and electrochemistry of 4'-functionalized 2,2':6',2''-terpyridine ruthenium(II) complexes and their biological activity. *Dalton Trans.* **16**, 2136–2143. (doi:10.1039/b716011a)
 69. Vougiouklakis GC, Stergiopoulos T, Kantonis G, Kontos AG, Papadopoulos K, Stublla A, Potvin PG, Falaras P. 2010 Terpyridine- and 2,6-dipyridinylpyridine-coordinated ruthenium (II) complexes: Synthesis, characterization and application in TiO₂-based dye-sensitized solar cells. *J. Photochem. Photobiol. A.* **214**, 22–32. (doi:10.1016/j.jphotochem.2010.06.001)
 70. Argazzi R, Laramona G, Contado C, Bignozzi CA. 2004 Preparation and photoelectrochemical characterization of a red sensitive osmium complex containing 4,4',4''-tricarboxy-2,2':6',2''-terpyridine and cyanide ligands. *J. Photochem. Photobiol. A* **164**, 15–21. (doi:10.1016/j.jphotochem.2003.12.016)
 71. Ashraf J *et al.* 2017 Design, synthesis and antibacterial activities of new azo-compounds: an experimental and a computational approach. *Letts. Drug Des. Discov.* **14**, 1145–1154. Available from: <http://www.rscb.org/pdb/home/> home do (last accessed on 15 July 2020)
 72. Hussain F, Khan Z, Jan MS, Ahmad S, Ahmad A, Rashid U, Ullah F, Ayaz M, Sadiq A. 2019 Synthesis, *in-vitro* α -glucosidase inhibition, antioxidant, *in-vivo* antidiabetic and molecular docking studies of pyrrolidine-2,5-dione and thiazolidine-2,4-dione derivatives. *Bioorg. Chem.* **91**, 103128. (doi:10.1016/j.bioorg.2019.103128)
 73. Muhammad SA, Fatima N. 2015 *In silico* analysis and molecular docking studies of potential angiotensin-converting enzyme inhibitor using quercetin glycosides. *Pharmacogn. Mag.* **11**, S123. (doi:10.4103/0973-1296.157712)
 74. Ashraf J *et al.* 2017 Design, synthesis and antibacterial activities of new azo-compounds: an experimental and a computational approach. *Letts. Drug Des. Discov.* **14**, 1145–1154. (doi:10.2174/1570180814666170306124134)
 75. Mughal EU *et al.* 2018 Design, synthesis and biological evaluation of novel

- dihydropyrimidine-2-thione derivatives as potent antimicrobial agents: experimental and molecular docking approach. *Letts. Drug Des. Discov.* **15**, 1189–1201. (doi:10.2174/1570180815666180209151516)
76. Te Velde GT, Bickelhaupt FM, Baerends EJ, Fonseca Guerra C, Van Gisbergen SJ, Snijders JG, Ziegler T. 2001 Chemistry with ADF. *J. Comput. Chem.* **22**, 931–967. (doi:10.1002/jcc.1056)
77. Li J, Liu R, Jiang J, Liang X, Huang L, Huang G, Chen H, Pan L, Ma Z. 2019 Zinc(II) terpyridine complexes: Substituent effect on photoluminescence, antiproliferative activity, and DNA interaction. *Molecules.* **24**, 4519. (doi:10.3390/molecules24244519)
78. Karges J, Blacque O, Jakubaszek M, Goud B, Goldner P, Gasser G. 2019 Systematic investigation of the antiproliferative activity of a series of ruthenium terpyridine complexes. *J. Inorg. Biochem.* **198**, 110752. (doi:10.1016/j.jinorgbio.2019.110752)
79. Anthonyamy A, Balasubramanian S, Chinnakali K, Fun HK. 2007 4'-(4-Methoxyphenyl)-2,2':6',2''-terpyridine. *Acta Cryst.* **63**, 1148–1150.
80. Movassagh B, Yousefi A, Momeni BZ, Heydari S. 2014 A general and highly efficient protocol for the synthesis of chalcogenoacetylenes by copper (I)-terpyridine catalyst. *Synlett.* **25**, 1385–1390. (doi:10.1055/s-0033-1341277)
81. Ledwaba P, Munro OQ, Stewart K. 2009 4'-[2-(Trifluoromethyl)phenyl]-2,2':6',2''-terpyridine. *Acta Cryst.* **65**, 376–377.
82. Fu WW, Zhang FX, Kuang DZ. 2014 Syntheses and crystal structures of [Fe(*m*-NO₂phtpy)₂](ClO₄)₂ and [Fe(*m*-Clphtpy)₂](ClO₄)₂ (*m*-NO₂phtpy = 4'-(3-nitrophenyl)-2,2':6',2''-terpyridine and *m*-Clphtpy = 4'-(3-chlorophenyl)-2,2':6',2''-terpyridine). *J. Struct. Chem.* **55**, 895–900. (doi:10.1134/S002247661405014X)
83. Sumra SH *et al.* 2018 Metal based triazole compounds: their synthesis, computational, antioxidant, enzyme inhibition and antimicrobial properties. *J. Mol. Struct.* **1168**, 202–211. (doi:10.1016/j.molstruc.2018.05.036)
84. Aihara JI. 1999 Reduced HOMO–LUMO gap as an index of kinetic stability for polycyclic aromatic hydrocarbons. *J. Phy. Chem. A* **103**, 7487–7495. (doi:10.1021/jp990092i)
85. Balachandran V, Lakshmi A, Janaki A. 2012 Conformational stability, vibrational spectral studies, HOMO–LUMO and NBO analyses of 2-hydroxy-4-methyl-3-nitropyridine and 2-hydroxy-4-methyl-5-nitropyridine based on density functional theory. *J. Mol. Struct.* **1013**, 75–85. (doi:10.1016/j.molstruc.2012.01.021)
86. Sharma Y. 2007 *Elementary organic spectroscopy*. New Delhi, India: S. Chand Publishing.
87. Parr RG, Szentpaly LV, Liu S. 1999 Electrophilicity index. *J. Am. Chem. Soc.* **121**, 1922–1924. (doi:10.1021/ja983494x)
88. Arjunan V, Saravanan I, Ravindran P, Mohan S. 2009 Structural, vibrational and DFT studies on 2-chloro-1H-isoindole-1,3(2H)-dione and 2-methyl-1H-isoindole-1,3(2H)-dione. *Spectrochim. Acta A.* **74**, 642–649. (doi:10.1016/j.saa.2009.07.012)
89. Suresh D, Amalanathan M, Sebastian S, Sajan D, Joe IH, Jothy VB, Nemeç I. 2013 Vibrational spectral investigation and natural bond orbital analysis of pharmaceutical compound 7-amino-2,4-dimethylquinolinium formate–DFT approach. *Spectrochim. Acta A* **115**, 595–602. (doi:10.1016/j.saa.2013.06.077)